Am J Cancer Res 2021;11(3):712-728
www.ajcr.us /ISSN:2156-6976/ajcr0122299

Original Article

FSTL1 promotes growth and metastasis in gastric cancer by activating AKT related pathway and predicts poor survival

Mengjie Wu[1,2*], Yongfeng Ding[2*], Nan Wu[3*], Junjie Jiang[2], Yingying Huang[2], Fanyu Zhang[4], Haiyong Wang[2], Quan Zhou[2], Yan Yang[2], Wei Zhuo[5], Lisong Teng[2]

[1]Department of Medical Oncology, Affiliated Cancer Hospital of Zhengzhou University, Henan Cancer Hospital, Zhengzhou 450008, Henan, P. R. China; [2]The First Affiliated Hospital, Zhejiang University School of Medicine, Hangzhou, Zhejiang, P. R. China; [3]Department of Thoracic Surgery, First Affiliated Hospital of Zhengzhou University, Zhengzhou, Henan, P. R. China; [4]College of Basic Medicine, Zhengzhou University, Zhengzhou, Henan, P. R. China; [5]Department of Cell Biology, Zhejiang University School of Medicine, Hangzhou, P. R. China. [*]Equal contributors.

Received September 13, 2020; Accepted December 8, 2020; Epub March 1, 2021; Published March 15, 2021

Abstract: Accumulating evidence on the role of Follistatin-like protein 1 (FSTL1) in tumorigenesis and cancer progression is conflicting. Nevertheless, the underlying mechanisms by which FSTL1 contributes to gastric cancer (GC) remain unknown. This study shows that FSTL1 was frequently upregulated in primary GC tissues and significantly correlated with infiltrating depth, lymph node metastasis, unfavorable tumor stage and poor prognosis of GC. Down or up-regulation of FSTL1 inhibited or increased, respectively, the proliferation by reducing apoptosis, clonogenicity, migration and invasion of GC cells *in vitro*. Moreover, the higher expression of FSTL1 promoted subcutaneous xenograft tumor growth and lung/liver tumor metastasis *in vivo*. Furthermore, we demonstrate that FSTL1 is involved in regulation of the AKT signaling through analyzing databases and experimental results. Mechanistic studies showed that FSTL1 promoted proliferation, migration and invasion in GC, at least partially, by activating AKT via regulating TLR4/CD14. In all, this study highlights the role of the FSTL1-TLR4/CD14-AKT axis, which provided novel insights into the mechanism of growth and metastasis in GC for the first time.

Keywords: Gastric cancer, FSTL1, TLR4/CD14, AKT, prognosis

Introduction

Gastric cancer (GC), one of the most common malignant tumors, is a leading cause of cancer-related mortality, especially in China [1, 2]. Despite the improvement in the current diagnosis and therapeutics, a low 5-year survival rate of GC patients at an advanced stage, owing to late presentation, high recurrence and metastasis rate, remains a challenge [3]. Therefore, it is critical to unveil the molecular mechanisms of GC and find a specific biomarker for diagnosis and prognosis to improve the clinical management of advanced GC.

AKT, a serine and threonine kinase, plays a pivotal role in cancer formation and progression. Upon its activation, AKT can regulate numerous downstream targets, such as the Bcl2 family, FAK and snail, with various functions including cell growth, survival, apoptosis, migration and transformation [4]. The Bcl2 family, one of AKT downstream signaling targets, comprises activators (Bax, Bid, Bim) or inhibitor (Bcl2, Bcl-xl, Mcl1) of apoptosis, which plays an essential part in regulating cell apoptosis [5]. Akt mediates the interaction of 14-3-3 proteins and phosphorylated BAD, and thereby regulating the anti-apoptotic function of Bcl2 and Bcl-xl [6]. Furthermore, emerging evidence indicate that AKT associated signaling pathway contributes to the motility and invasion of malignant cells. The activation of AKT-FAK signaling is responsible for cancer metastasis via regulating the adhesion of epithelial cancer cells to extracellular matrix proteins [7]. AKT-snail pathway mediated epithelial to mesenchymal transition also regulates migration of tumor cells [8]. However, the key upstream factor that links AKT

signaling and GC malignant progression remain largely unknown.

Follistatin-like protein 1 (FSTL1), also named as transforming growth factor (TGF)-β-induced clone 36 (TSC36) or follistatin-related protein (FRP), is a 308 amino acid secreted glycoprotein belonging to the osteonectin (SPARC) family. It contains a pair of EF-hand domains, a follistatin-like domain, and a VMFC domain [9]. Studies have shown that FSTL1 is mainly involved in systemic autoimmune disease, developmental processes, and cardiovascular diseases [10-12]. Although emerging evidence suggests a close association between FSTL1 and the development and progression of various cancer, it is controversial [11]. FSTL1 was reported to suppress tumor growth, migration, and invasiveness in ovarian, lung, endometrial, and nasopharyngeal carcinoma [13-17]. On the other hand, FSTL1 was upregulated in hepatocellular carcinoma (HCC), esophageal squamous cell carcinoma (ESCC), breast cancer, and colon cancer. Yang W et al. showed that overexpression of FSTL1 in HCC promoted proliferation and inhibited apoptosis by activating the AKT/GSK-3β pathway [18]. Similarly, FSTL1 promoted chemoresistance and metastasis via NF-kB-BMP crosstalk in ESCC [19]. To date, only one study showed that the expression of FSTL1 was upregulated in GC cell lines and FSTL-1 knockdown may promoted GC cell apoptosis via the STAT6 signaling pathway [20]. The clinical significance of FSTL1 and its associated molecular mechanism in GC development and progression require further in-depth study.

In this study, the expression profile and clinical significance of FSTL1 and its correlations with GC patient survival were investigated by analyzing multiple public databases and clinical samples. We demonstrated that FSTL1 contributed to the growth and metastasis of GC *in vivo* and in *vitro*. Importantly, FSTL1 promoted proliferation, migration, and invasion in GC, at least partially, by activating AKT via regulating TLR4/CD14, which provided novel insights into the molecular mechanism of FSTL1 in GC pathogenesis.

Materials and methods

Clinical samples

A total of primary GC and matched non-tumor tissue samples (Zhejiang cohort 1 N = 108 for qPCR; Zhejiang cohort 2 N = 30 for western blot; Zhejiang cohort 3 N = 106 for IHC) were collected from patients referred to the Zhejiang University, who provided written informed consent prior to surgical resection. Patients were diagnosed with GC based on histopathology and had not received adjuvant treatment before surgery. Tumor staging was determined according to the American Joint Committee on Cancer (eighth edition).

Cell lines and transfection

Five human GC cell lines (HGC27, SGC7901, BGC823, MKN45, and MKN28) were cultured in RPMI 1640 (Gibco, Rockville, MD, USA) supplemented with 10% fetal bovine serum (FBS; Gibco). All cell lines were purchased from the Shanghai Cell Bank of Chinese Academy of Sciences (Shanghai, China).

Human FSTL1 expression was knocked down using a specific FSTL1 siRNA (siFSTL1) or short-hairpin plasmids (shFSTL1), which were purchased from Sigma (Shanghai, China). These two siRNAs sequences were: siFSTL1-1, sense, GAAGAGCUAAGGAGCAAAUTT, antisense, AUUUGCUCCUUAGCUCUUCTT; siFSTL1-2, sense, GAGCAAUGCAAACCUCACATT, antisense, UGUGAGGUUUGCAUUGCUCTT. Plasmids and sequences of shRNAs were: shFSTL1-1 (pGpU6/Neo, GCCTGTGTGTGGCAGTAATGG), shFSTL1-2 (pGpU6/Neo, GCTGGAAGCTGAGATCATTCC). Expression of human FSTL1 was upregulated using a plasmid (pEX-3) for cell assays (Sigma, Shanghai, China) or a lentiviral vector (GV492, FSTL1 (NM_007085)) for animal assays (ov-FSTL1 and ov-NC) (Gene, Shanghai, China). siRNA and plasmids were transfected with Lipofectamine 3000 transfection reagent (Invitrogen, Carlsbad, California, USA) in Opti-MEM medium (Gibco, Carlsbad, California, USA) according to the manufacturer's instructions.

Quantitative real-time PCR (qRT-PCR)

Detailed method for RT-qPCR is given in the Supplementary Methods.

Immunohistochemistry (IHC)

Detailed method for IHC assay is in the Supplementary Methods.

Cell proliferation, apoptosis, and transwell assay

Detailed methods for cell proliferation, apoptosis and transwell assay are given in the Supplementary Method.

Co-immunoprecipitation (co-ip)

Co-ip experiments were performed using the Crosslink Magnetic IP/Co-IP Kit (Thermo Scientific, America). Briefly, FSTL1 antibody (5 ug, Proteintech) was bound to Protein A/G magnetic beads for 15 minutes, crosslink antibody to beads with DSS for 30 minutes, and then incubate cell lysate with prepared beads overnight at 4°C. Finally, immunoprecipitated proteins were separated by SDS-PAGE, and visualized by Western blot.

Immunofluorescence

Cells were seeded on glass coverslips and cultured for 24 hours and fixed with 4% Polyoxymethylene for 15 minutes at room temperature. After permeabilization with 0.1% Triton X-100 for 25 minutes at room temperature, cells were blocked in 10% normal blocking serum at 37°C for 30 min, and incubated with primary antibodies against FSTL1 (10 ug/ml, AF1694, R&D) and TLR4 (1:50, ab13556, Abcam), and CD14 (1:50, ab181470, abcam) overnight at 4°C, followed by incubation with 557-conjugated Anti-Goat IgG Secondary Antibody (1:1000, NL001, R&D) or 488-conjugated anti-Rabbit IgG secondary antibodies (1:1000, #4412, CST) or 647-conjugated anti-mouse IgG secondary antibodies (1:1000, ab6563, Abcam) for 1 hour at room temperature. To visualize the nuclei, cells were stained with 6-diamidino-2-phenylindole (DAPI; 1 ug/ml; Sigma-Aldrich, USA).

Western blot

Detailed methods for western blotting is described in the Supplementary Methods. For collection of conditioned medium from GC cell lines, cells were first serum-starved for 24 hours and conditioned medium was subsequently collected.

In vivo xenograft models

Male athymic nude mice (BALB/C, 3-4 weeks) aged 3-4 weeks were purchased from Nanjing Provincial Center for Disease Control and Prevention. All animal experiments were approved by the Institutional Animal Care and Use Committee at the Zhejiang University. For xenograft models, 7×10^6 HGC-27 or BGC823 cells stably transfected with ov-FSTL1 vector or ov-NC were injected subcutaneously in the right flank of mice (five mice per group). Tumor size in mice was measured every 7 days. Tumor volumes were calculated using the formula: $V\ (mm^3) = 0.5 \times a \times b^2$ (V, volume; a, longitudinal diameter; b, latitudinal diameter). After 5 weeks, these mice were sacrificed, tumors were weighed, and processed for hematoxylin and eosin staining.

2×10^6 BGC823 cells transfected with ov-FSTL1 or ov-NC were intravenously injected through tail vein into nude mice to study tumor metastasis *in vivo*. After 6 weeks, mice were sacrificed and lungs and livers were harvested for tumor nodules and IHC.

Bioinformatics

mRNA expression of FSTL1 in GC and clinical information of GC patients was analyzed by using data from the Cancer Genome Atlas (TCGA) (https://cancergenome.nih.gov) and Oncomine database (https://www.oncomine.org). The gene expression data and patients clinicopathological information was download from the TCGA via cBioPortal (https://www.cbioportal.org/) (on 4 November 2018).

The Kaplan-Meier (K-M) plotter database (http://kmplot.com/analysis/) was investigated to validate the prognostic value of FSTL1. GC patients were divided into two cohorts based on FSTL1 expression (high vs. low expression). The overall survival (OS) and progression-free survival (PFS) of GC patients were analyzed in K-M plotter database. Log rank *p*-value and samples counts were calculated.

Genes co-expressing with FSTL1 in GC were identified in the cBioPortal for Cancer Genomics (http://www.cbioportal.org/) and the Coexpedia (http://www.coexpedia.org/index.php). Co-expressed genes in cBioPortal were extracted based on a |Pearson's r| ≥ 0.4 and |Spearman's r| ≥ 0.4. Genes overlapping both in cBioPortal and Coexpedia were used for gene ontology (GO) and Kyoto Encyclopedia of Genes and Genomes (KEGG) pathway analysis in David v6.7 (http://david.abcc.ncifcrf.gov/) to elucidate enrichment in biological processes and signaling pathways.

Statistical analysis

Data were presented as mean ± standard deviation. Two or multiple groups were compared

using t-test and one-way ANOVA, respectively. *P* value < 0.05 was considered statistically significant (*P < 0.05, **P < 0.01, ***P < 0.001). Chi-square and Yates' continuity corrected chi-square tests were used to analyze categorical data. Survival rates were calculated using the Kaplan-Meier method, and the difference between curves was analyzed using Log-rank test. Univariate and multivariate analysis were performed using the Cox regression model. Variables with P < 0.05 were included in the multivariate analysis to identify independent factor. Western blot band intensity was analyzed by Image J. RNA fluorescence in situ hybridization images were analyzed by FV10-ASW software. Statistical analysis was performed using GraphPad Prism 8 software.

Results

FSTL1 is upregulated and correlated with poor prognosis in GC

FSTL1 expression in GC was firstly extracted from the TCGA, Oncomine databases and results showed FSTL1 mRNA in GC was upregulated and its expression was higher in stage II-IV samples than stage I (**Figures 1A** and S1A). This was validated in Zhejiang cohort 1 (108 GC tissues and paired normal tissues) (**Figure 1B**). Then the expression of FSTL1 protein was next analyzed by western blot and IHC in paired tumor tissues and corresponding normal tissues of Zhejiang cohort 2 and 3. Results showed that FSTL1 level was elevated in GC and its expression was higher in stage III-IV than stage I-II (**Figures 1C-F** and S1B). In addition, upregulation of FSTL1 was significantly correlated with the infiltrating depth, lymph node metastasis, and unfavorable tumor stage of GC in TCGA database and Zhejiang cohorts 1 and 3 (**Tables 1** and S1, S2). As shown in **Figure 2A**, GC patients with overexpressing FSTL1 in K-M plotter, TCGA databases and Zhejiang cohort 3 had remarkably shorter overall survival (OS) compared to patients with low FSTL1 expression. Meanwhile, high FSTL1 level in GC was correlated with poor prognosis of PFS in K-M plotter (Figure S2A). Further stratification according to the clinical characteristics of GC patients in K-M plotter showed that high expression of FSTL1 was significantly associated with poor OS and PFS in TNM stage III and IV patients and patients with lymph node metastasis (stage N1-3), but not in stage I and II or stage N0, indicating FSTL1 was prognostic in advanced stages and lymph node metastasis (**Figures 2B-E**, S2B-D and Table S3). Also, multivariate analysis in Zhejiang cohort 3 showed that FSTL1 expression was an independent prognostic factors for OS (**Figure 2F**). Collectively, these data suggested that FSTL1 was aberrantly upregulated and associated with poor prognosis in GC, especially in the advanced stages.

FSTL1 promotes GC cells proliferation, migration and invasion in vitro

Previously, Marco et al. reported that FSTL1, as a secretory protein, was detected in condition medium of ESCC cells. Therefore, endogenous mRNA expression of FSTL1, and protein levels of five GC cell lines (SGC7901, BGC823, HGC27, MKN28 and MKN45) were measured (Figure S3A). To investigate the role of FSTL1 on the biological behavior of GC cells, we silenced FSTL1 expression using siRNA or shRNA in GC cells: SGC7901 cells were transfected with siFSTL1-1/siFSTL1-2 and normal control (siNC); HGC27 cells were transfected with shFSTL1-1/shFSTL1-2 and control (shNC). Successful knockdown of FSTL1 in GC cells was confirmed by qRT-PCR and western blotting (Figure S3B, S3C). Silencing FSTL1 by siRNA or shRNA decreased the rate of proliferation in GC cells (**Figure 3A**). Colony formation capacity was decreased in both siFSTL1 and shFSTL1 transfected GC cell lines compared to the respective controls (**Figures 3B** and S3D). Furthermore, silencing FSTL1 increased the proportion of apoptotic cells compared with NC groups (**Figure 3C**) indicating that down-regulation of FSTL1 promoted apoptosis, and thus inhibition of cell proliferation. Moreover, suppression of FSTL1 attenuated migration and invasiveness of SGC7901 and HGC27 cells (**Figure 3D**, **3E**).

In addition, we also analyzed the effect of FSTL1 overexpression on the growth and motility of GC cells. Over-expression of FSTL1 expression in HGC27 and BGC823 cells was confirmed by western blotting (Figure S3E, S3F). Over-expression of FSTL1 enhanced proliferation, colony formation, migration and invasiveness of HGC27 and BGC823 cells, and significantly reduced apoptosis of the GC cells (**Figures 4A-E** and S3G-I). Expression apoptosis related inhibited proteins (Mcl1, Bcl2, Bcl-xl)

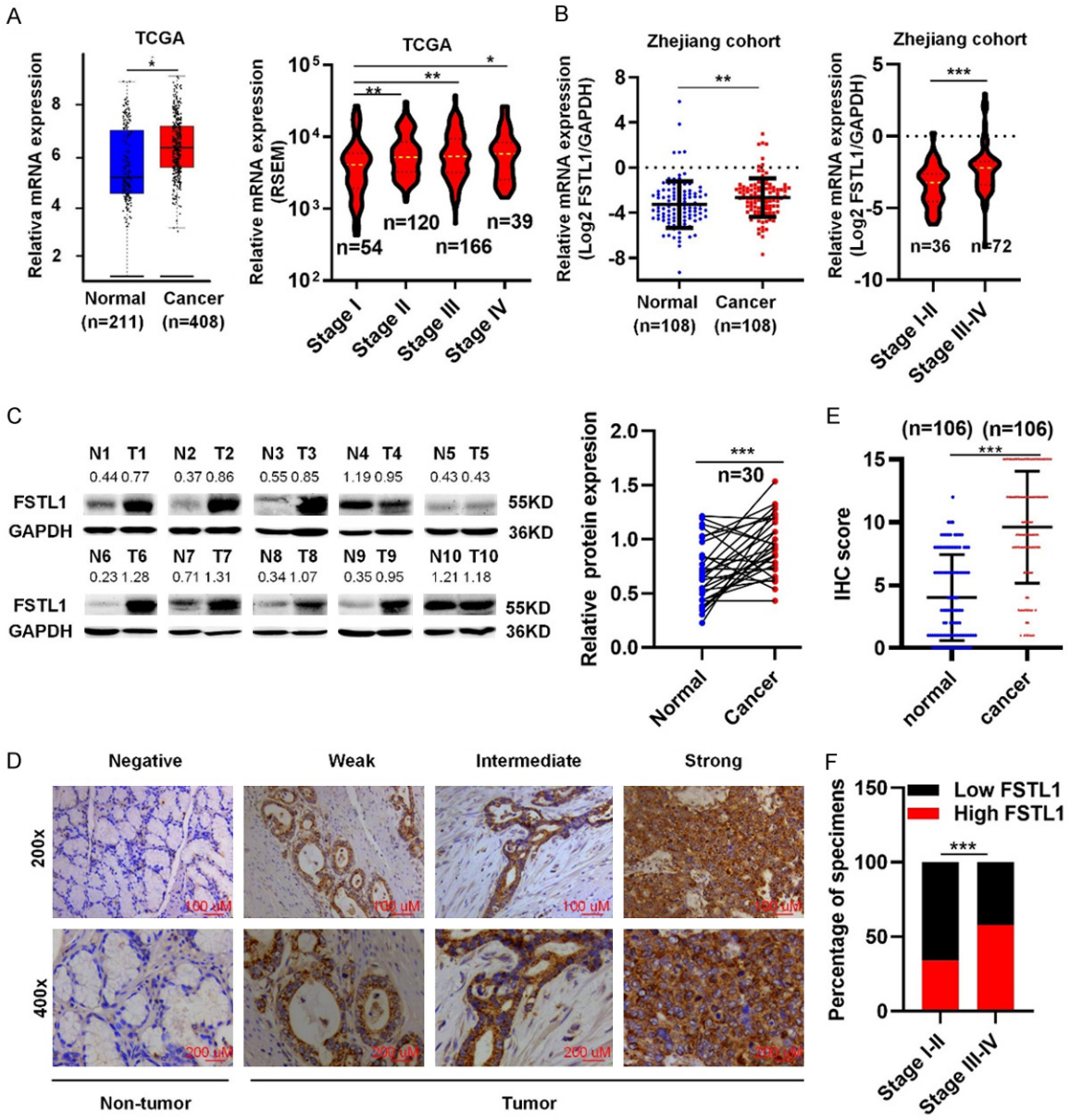

Figure 1. FSTL1 is overexpressed in GC. A. FSTL1 mRNA levels in GC and normal gastric tissue in TCGA database (Data from GEPIA: http://gepia.cancer-pku.cn; Match TCGA normal and GTEx data) and the mRNA expression of FSTL1 at stage I-IV of GC in TCGA database. B. FSTL1 mRNA levels in GC and normal gastric tissue and the mRNA expression of FSTL1 at stage I-II and III-IV of GC in Zhejiang cohort 1. C. Representative images of FSTL1 proteins level in Zhejiang cohort 2 (Sample 1-10). D, E. IHC analysis of FSTL1 in Zhejiang cohort 3 (SP, × 200). F. The percentage of FSTL1 at stage I-II and stage III-IV of GC in Zhejiang cohort 3. Data are shown as mean ± standard deviation. *P < 0.05, **P < 0.01, ***P < 0.001.

and metastasis associated proteins (p-FAK, FAK, EGFR, Snail1) were distinctly increased in response to FSTL1 overexpression in HGC27 and BGC823 cells, while the pro-apoptosis related proteins (Bax, Bim) were dramatically decreased compared with control vector groups (**Figure 4D** and **4F**). Overall, these data demonstrated that FSTL1 expression promoted GC cells proliferation, migration and invasion in vitro.

FSTL1 promotes gastric cancer cell tumorigenesis and metastasis in vivo

To examined whether FSTL1 could promote GC cells tumorigenesis and/or metastasis *in vivo*,

Table 1. Association between FSTL1 expression and clinicopathological features of GC in Zhejiang cohort 3

	No. patients	Low expression (n = 53)	High expression (n = 53)	*P* value
Gender				
Male	83 (78.3%)	41 (38.7%)	42 (39.6%)	0.8137[a]
Female	23 (21.7%)	12 (11.3%)	11 (10.4%)	
Age				
≤ 60	44 (41.5%)	20 (18.9%)	24 (22.6%)	0.4304[a]
> 60	62 (58.5%)	33 (31.1%)	29 (27.4%)	
Grade				
G1-2	9 (8.5%)	6 (5.7%)	3 (2.8%)	0.4895[b]
G3	97 (91.5%)	47 (44.3%)	50 (47.2%)	
T stage				
T1-2	15 (14.2%)	12 (11.3%)	3 (2.8%)	0.0258[b]
T3-4	91 (85.8%)	41 (38.7%)	50 (47.2%)	
N stage				
N0	21 (19.8%)	15 (14.1%)	6 (5.7%)	0.0283[a]
N1-3	85 (80.2%)	38 (35.8%)	47 (44.3%)	
M stage				
M0	89 (84%)	48 (45.2%)	41 (38.7%)	0.0639[a]
M1	17 (16%)	5 (4.7%)	12 (11.3%)	
Tumor size				
≤ 5 cm	60 (56.6%)	34 (32.1%)	26 (24.5%)	0.1169[a]
> 5 cm	46 (43.4%)	19 (17.9%)	27 (25.5%)	
AJCC stage				
I-II	30 (28.3%)	20 (18.9%)	10 (9.4%)	0.0311[a]
III-IV	76 (71.7%)	33 (31.1%)	43 (40.6%)	

[a]Chi-square test, [b]Yates' continuity corrected chi-square test.

HGC27 and BGC823 cells stably transfected with FSTL1 overexpression lentivirus vector (ov-FSTL1/ov-NC) (Figure S4) were implanted in nude mice. Five weeks after injection, tumor weights and volumes in the ov-FSTL1 group were significantly higher than the ov-NC group (**Figure 5A-F**). Importantly, consistent with these finding, HE staining showed histological feature of GC and IHC revealed that enhanced Ki-67 staining in ov-FSTL1 group than the ov-NC group, further supporting the notion that FSTL1 aids the proliferation and tumorigenicity of GC cells (**Figure 5G**). In addition, six weeks after intravenous injection of BGC823 cells through tail vein into nude mice, higher number of tumor nodules in the lungs and liver were found in ov-FSTL1 group compared with the ov-NC group, indicating FSTL1 induced GC cells metastasis (**Figure 5H**, **5I**). Taken together, these data revealed that FSTL1 promoted GC cell proliferation and metastasis *in vivo*.

Secretory FSTL1 promotes GC growth and metastasis by AKT activation

To better explore the molecular mechanisms of FSTL1-driven GC growth and progression, we selected the overlapping genes between cBioPortal and Coexpedia for GO and KEGG analyses in David v6.7 (http://david.abcc.ncifcrf.gov/) (Figure S5 and Tables S4, S5, S6). Signaling pathway analysis showed that FSTL1 was involved in AKT-associated signaling pathway (**Figure 6A**). Interestingly, FSTL1 knockdown reduced phosphorylation of AKT, while FSTL1 overexpression resulted in the activation of AKT (**Figure 6B**). As FSTL1 is a secretory glycoprotein, treating BGC823 cells with 1 ug/ml recFSTL1 protein (R&D Systems, 1694-FN-050) for 24 or 48 hours significantly increased the expression of phosphorylation of AKT, apoptosis related inhibited proteins (Mcl1, Bcl2, Bcl-xl), and metastasis associated proteins (p-FAK, EGFR, Snail1), decreased the expression of pro-apoptosis related proteins (Bax, Bim), indicating secretory FSTL1 may also play an important role in the progression of GC (**Figure 6C**). Inhibition of AKT by MK2206 (Selleck, USA) decreased phosphorylation of AKT and metastasis associated proteins, and rescued pro-apoptosis associated proteins resulting from elevated FSTL1 in BGC823 cells (**Figure 6D**). These results further confirmed that secretory FSTL1 enhanced GC cells growth and metastasis via regulating AKT-related signaling pathway.

FSTL1 activates AKT by partially regulating TLR4/CD14

Previous studies have shown that FSTL1 could bind to TLR4, CD14, Follistatin, or disco-interaction protein 2 homolog A (DIP2A) [21-23]. We found that in GC FSTL1 was tightly correlated with TLR4, CD14 and Follistatin expression, but not with DIP2A in TCGA (**Figure 7A**). A co-ip assay verified the interaction between TLR4, CD14 and FSTL1 in GC (**Figure 7B**). Meanwhile, correlation studies in 30 fresh frozen GC tis-

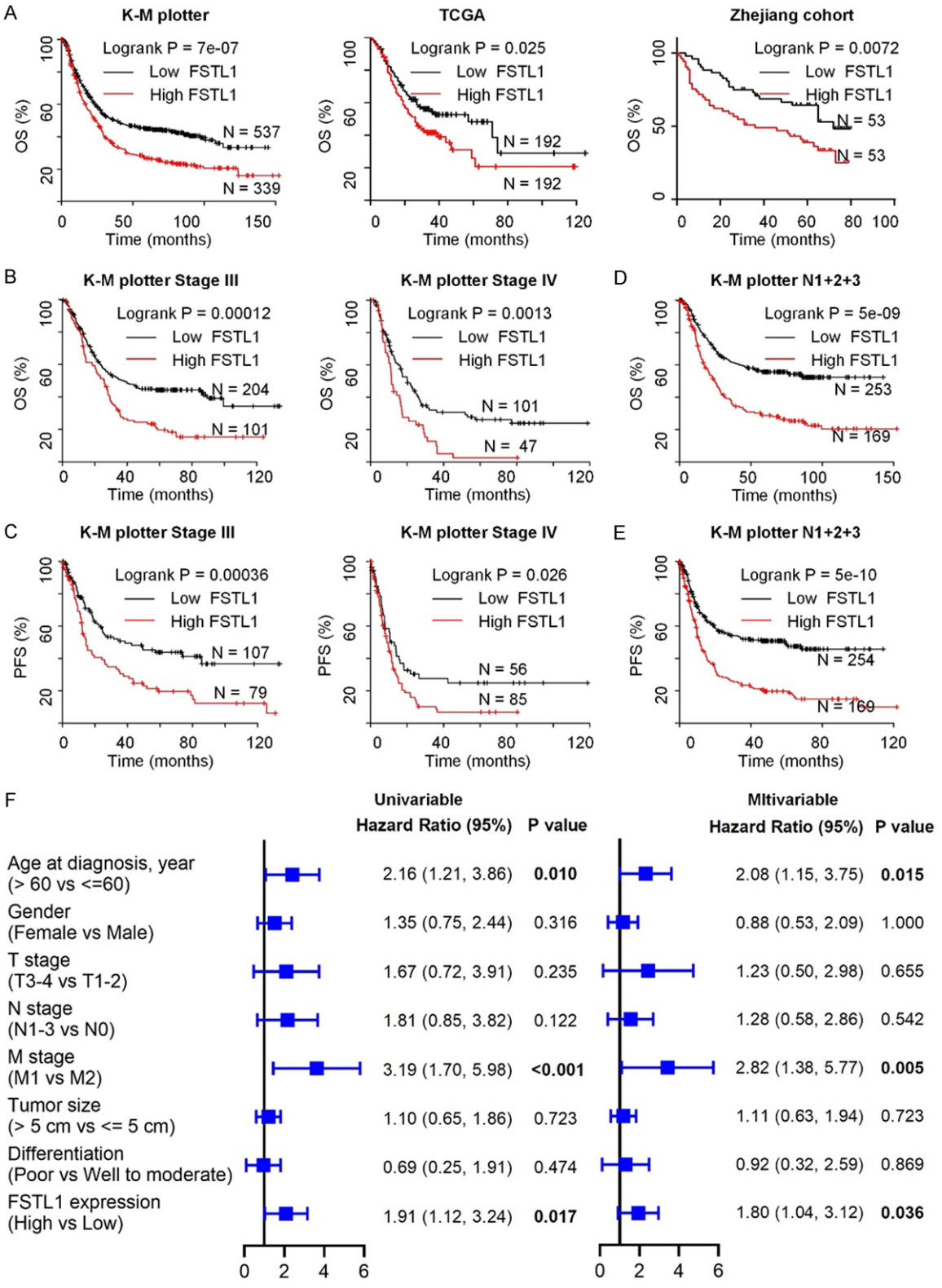

Figure 2. FSTL1 is associated with poor prognosis in GC. A. The association between FSTL1 expression and overall survival (OS) in GC patients assessed by K-M plotter, TCGA databases and Zhejiang cohort 3. B, C. Kaplan-Meier curves for OS and progression-free survival (PFS) of GC patients with stage III/IV using K-M plotter database. D, E. OS and PFS for GC patients with N1+2+3 disease. F. Univariable and multivariable analyses were performed in Zhejiang cohort 3. All the bars correspond to 95% confidence intervals.

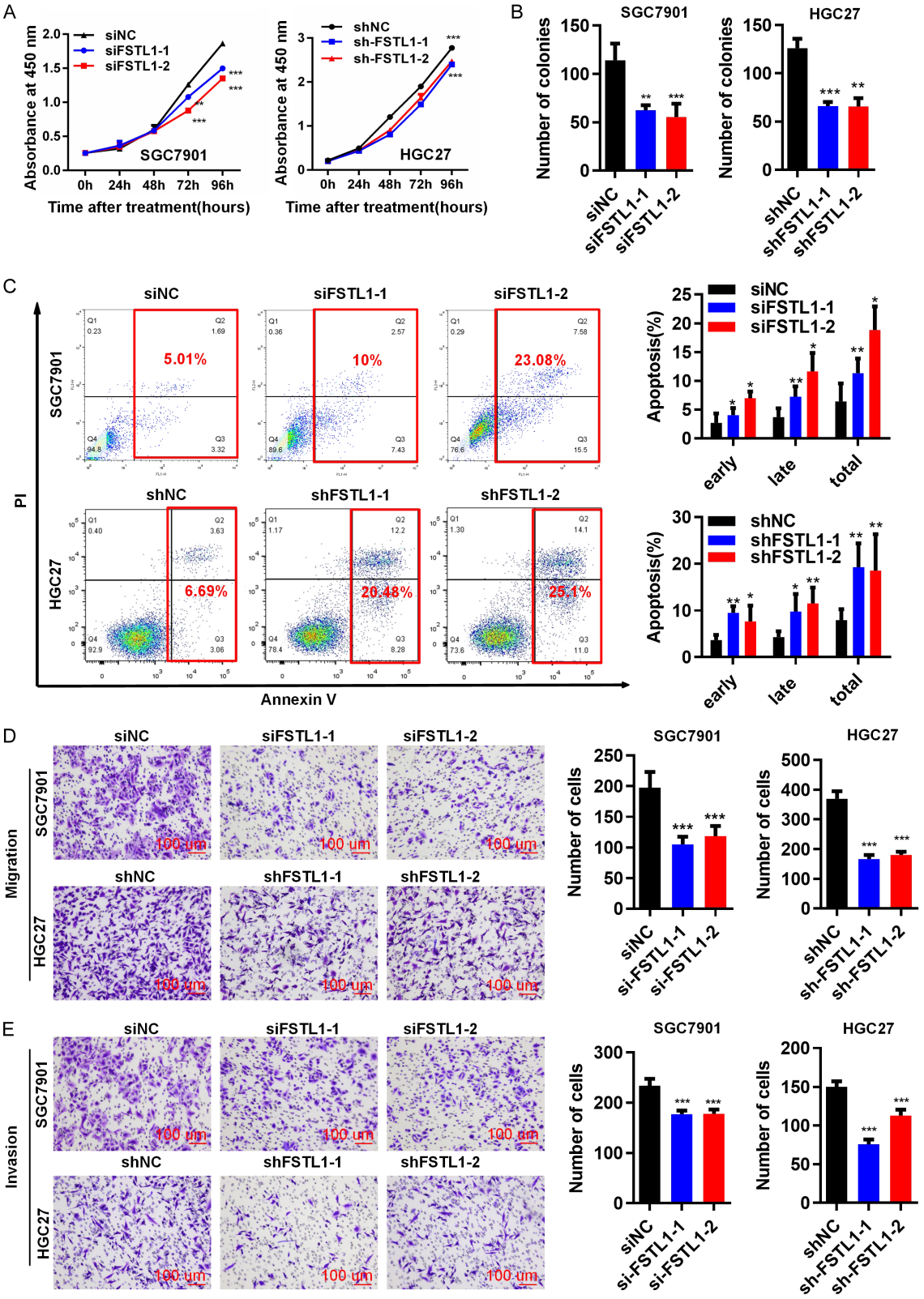

Figure 3. Silenced FSTL1 inhibits GC cells proliferation, migration and invasion *in vitro*. (A) CCK-8 assay, (B) Colony formation assay in SGC7901 and HGC27 cells transfected with siRNA/NC or shRNA/NC. (C) Flow cytometry analysis indicating the percentages of FSTL1 silenced and control cells at different apoptosis phases. (D) Migration assay, (E)

Invasion assay in SGC7901 and HGC27 cells transfected with siRNA/NC or shRNA/NC (SP, × 200). Representative images and the statistical analyses (mean ± standard deviation) were shown. *P < 0.05, **P < 0.01, ***P < 0.001.

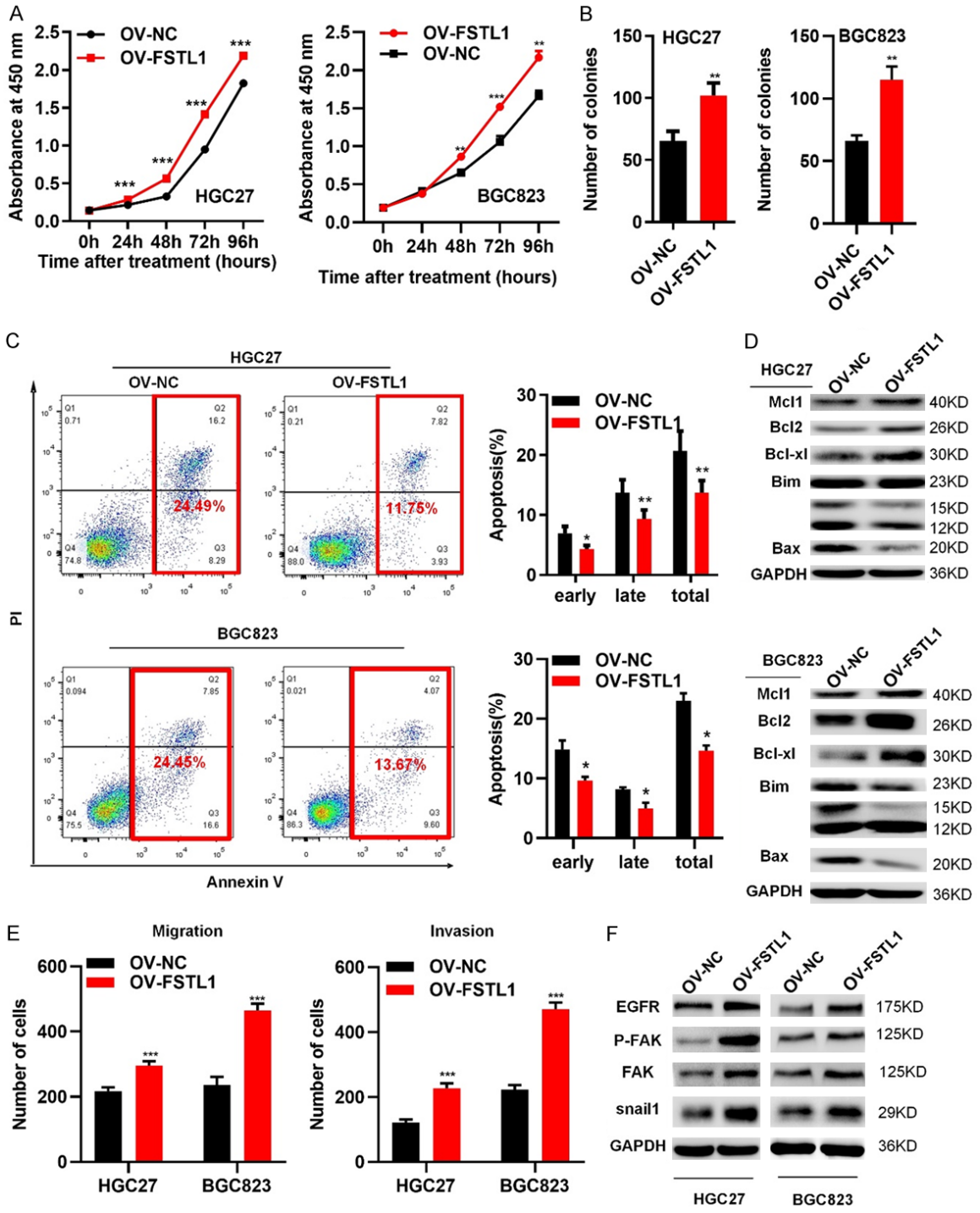

Figure 4. Overexpressed FSTL1 promotes GC cells proliferation, migration and invasion *in vitro*. (A) CCK8 assay, (B) Colony formation assay in HGC27 and BGC823 cells of overexpressing FSTL1/NC. (C) Flow cytometry showing the percentages of FSTL1 overexpressing cells and control cells at different apoptosis phases. (D) Apoptosis-associated proteins (Bim bands: 23 KD; 15 KD; 12 KD) in FSTL1 overexpressing cells by western blot. (E) Migration and invasion assay in HGC27 and BGC823 cells of elevating FSTL1. (F) Metastasis-correlated proteins in FSTL1 overexpressing cells by western blot. Representative images and the statistical analyses (mean ± standard deviation) were shown. *P < 0.05, **P < 0.01, ***P < 0.001.

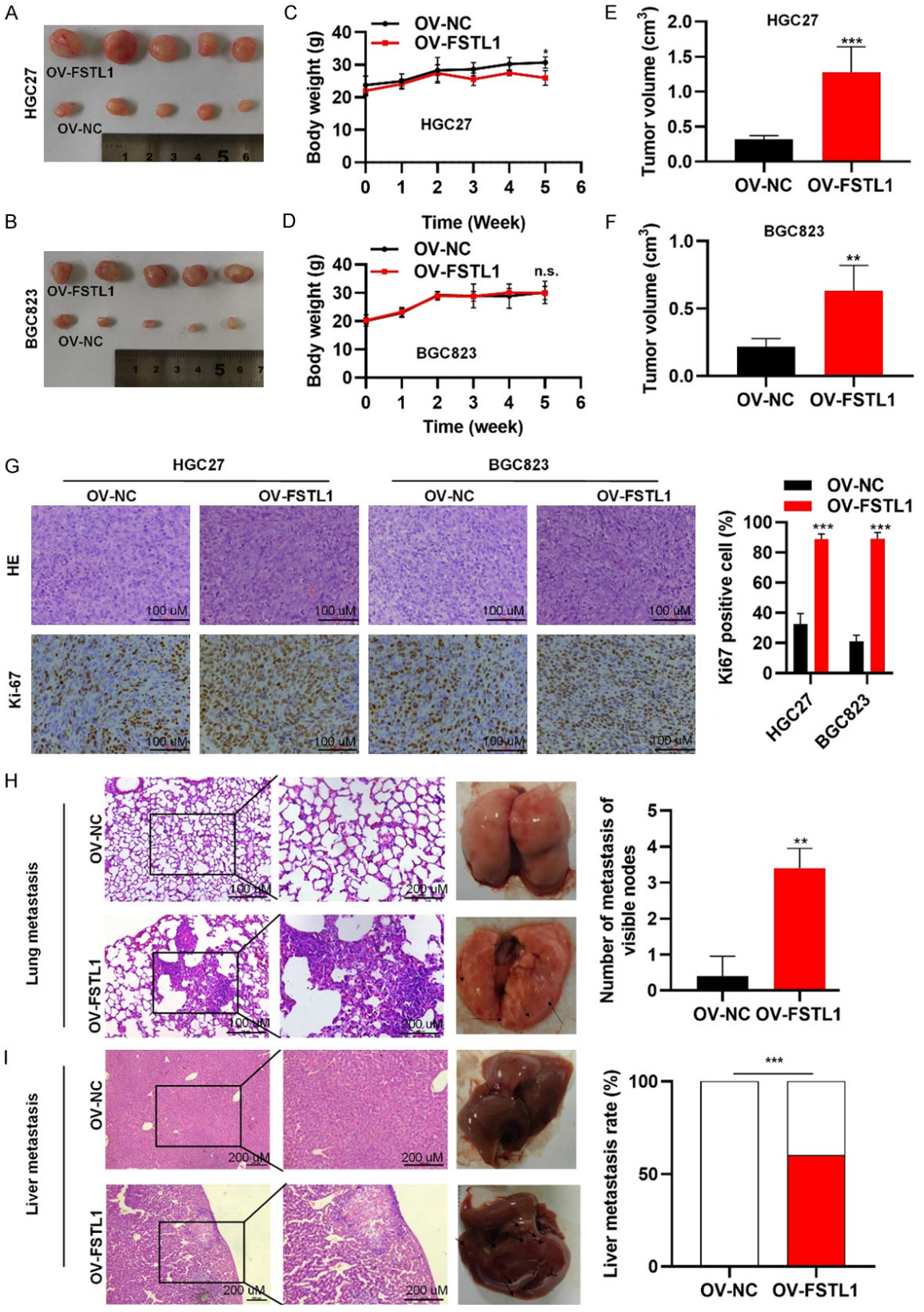

Figure 5. FSTL1 promotes gastric cancer cell tumorigenesis and metastasis *in vivo*. A, B. Representative images of subcutaneous tumors in nude mice injected with HGC27 and BGC823 cells transferred with stably OV-FSTL1/OV-NC. C-F. Tumor volumes and final body weights of nude mice injected with HGC27 and BGC823 cells transferred

with stably OV-FSTL1/OV-NC. G. HE staining and Ki-67 staining with anti-Ki67 antibody in xenografted HGC27 and BGC823 tumors overexpressing FSTL1. H, I. Representative images and HE staining of lung and liver metastases in nude mice by intravenous injection of BGC823 cells through tail vein. Data were expressed as mean ± standard deviation. *P < 0.05, **P < 0.01, ***P < 0.001. C-H. Based on Student's t-test. I. Based on Fisher's exact test.

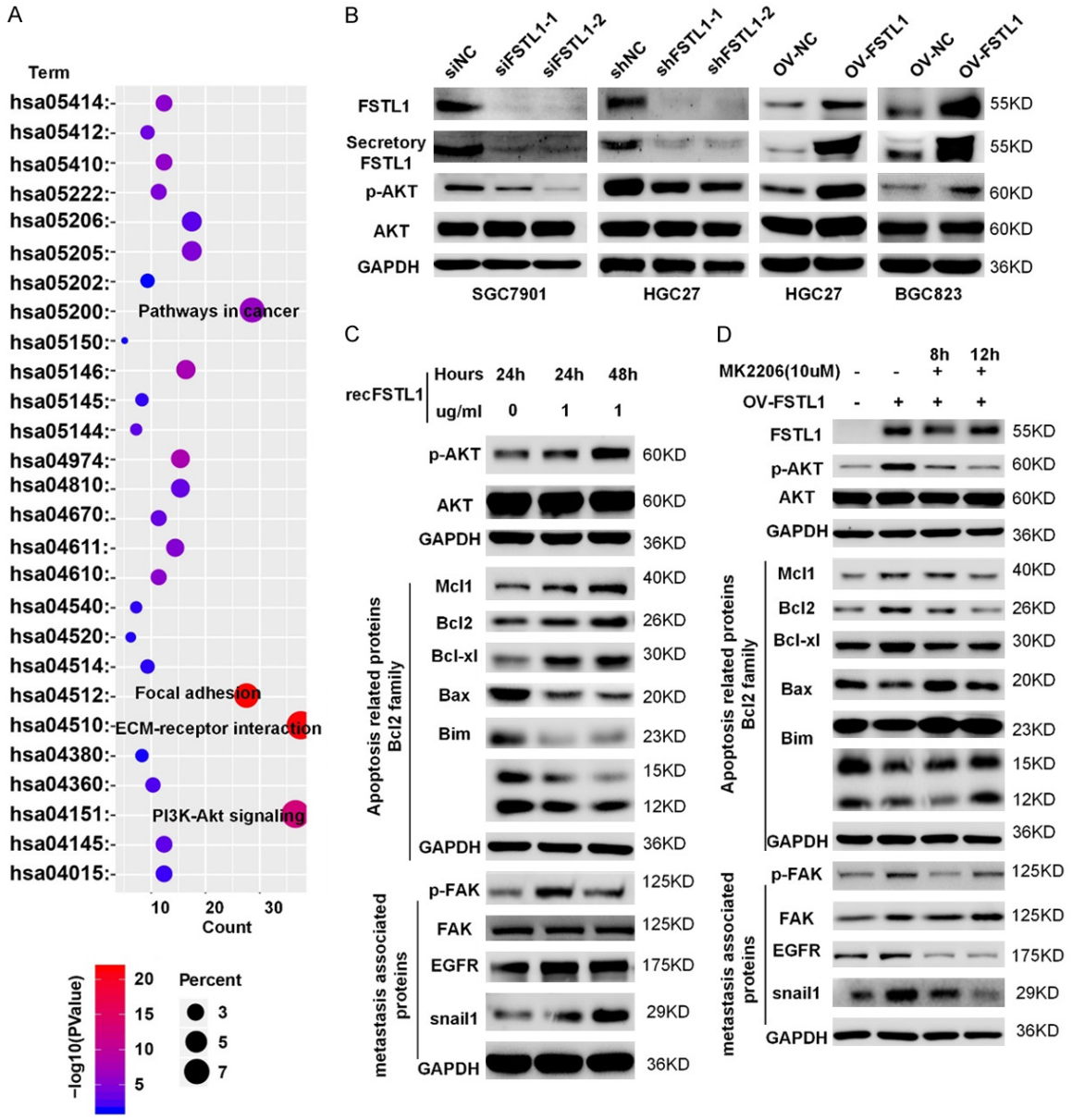

Figure 6. Secretory FSTL1 promotes GC growth and metastasis by AKT activation. A. KEGG pathway analysis of the genes significantly correlated with the FSTL1 expression in GC from cBioPortal and Coexpedia. KEGG, Kyoto Encyclopedia of Genes and Genomes. B. The protein expression levels of FSTL1, Secretory FSTL1, p-AKT and AKT in GC cell lines after FSTL1 silencing or overexpressing. C. The protein expression levels of p-AKT, AKT, apoptosis associated proteins (Bim bands: 23 KD; 15 KD; 12 KD) and metastasis related proteins in GC cell lines after the presence of recombinant FSTL1. D. The protein expression levels of p-AKT, AKT, apoptosis associated proteins (Bim bands: 23 KD; 15 KD; 12 KD) and metastasis related proteins in GC cell lines after the presence of recombinant FSTL1 and MK2206.

sues showed that FSTL1 mRNA expression was correlated positively correlated with TLR4, CD14 expression (**Figure 7C**). And similar results were received in the protein levels of 10 freshly GC tissues (**Figures 7D** and S6). Pervious study showed that TLR4 and CD14 complex is

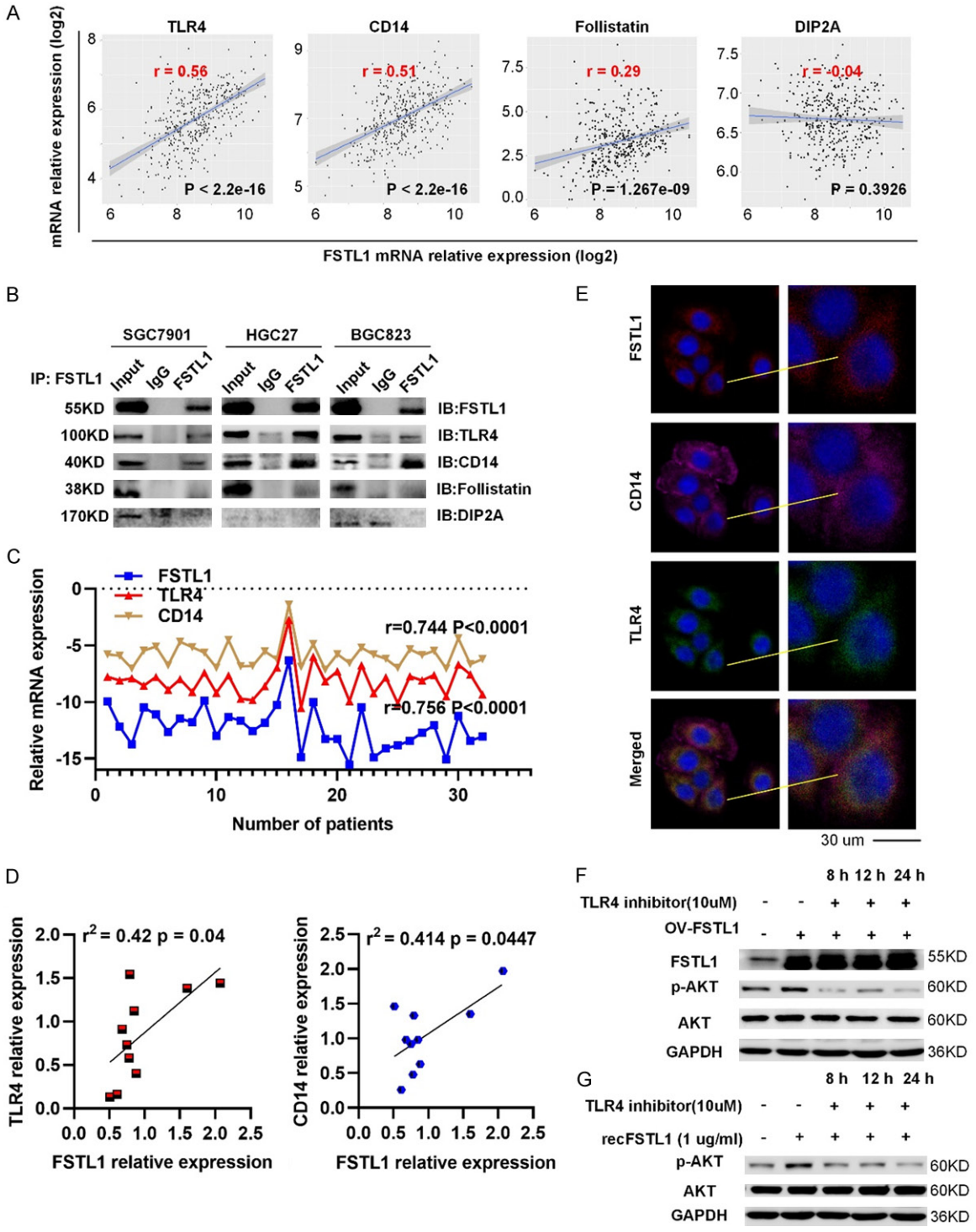

Figure 7. FSTL1 can promote the activation of AKT by regulating TLR4/CD14. A. Correlation analysis between TLR4/CD14/Follistatin/DIP2A expression and FSTL1 level in TCGA database. B. The physical interaction between TLR4, CD14, Follistatin, DIP2A and FSTL1 in SGC7901, HGC27 and BGC823 cells by co-immunoprecipitation. C. Correlation analysis between TLR4, CD14 mRNA expression and FSTL1 mRNA level in 30 fresh frozen GC tissues. D. Correlation analysis between TLR4, CD14 expression and FSTL1 level in 10 freshly GC tissues. E. Immunofluorescence images of TLR4, CD14, FSTL1 expression in SGC7901 cells. F, G. The protein expression levels of p-AKT, AKT proteins in BGC823 cells after overexpressed FSTL1 or the presence of recombinant FSTL1 and MK2206. A, C, D. Based on Spearman's rank correlation test.

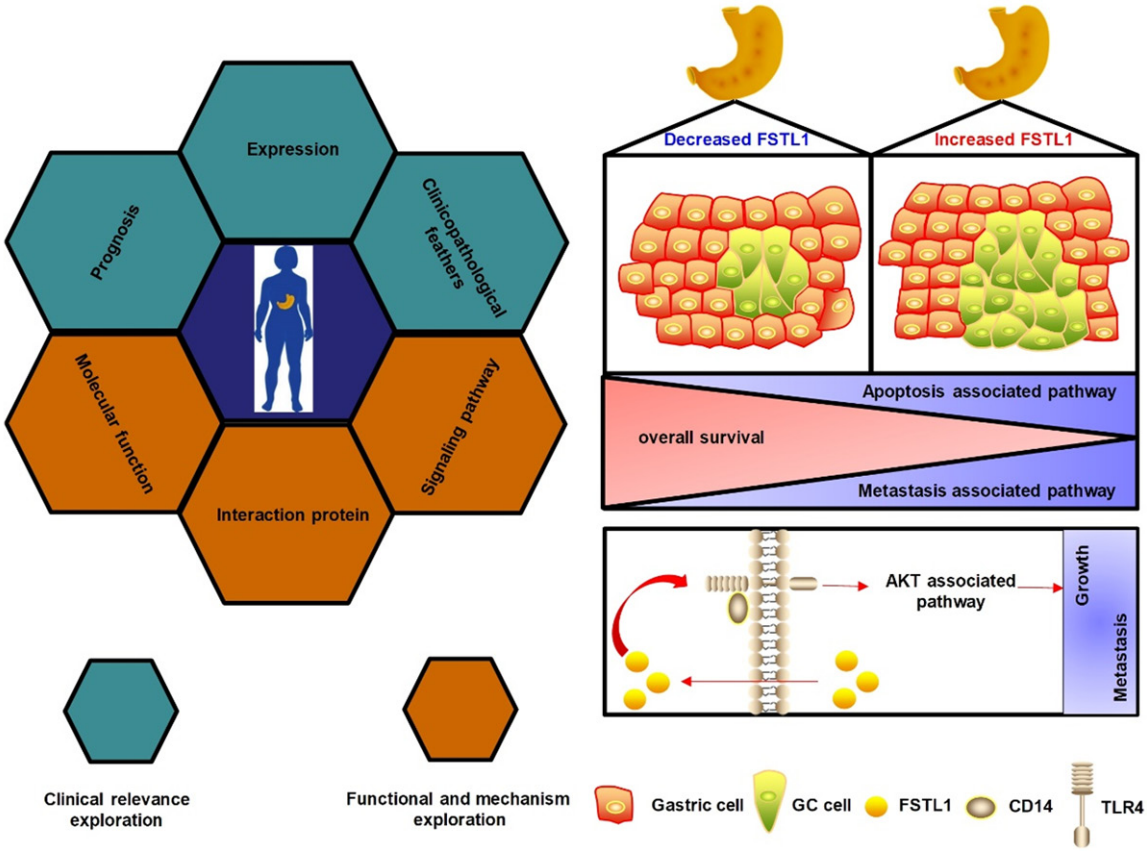

Figure 8. Schematic model of FSTL1-TLR4/CD14-AKT axis in GC. (Left) The integrative analytic strategy in this study. (Right) FSTL1 promotes growth and metastasis in GC by activating AKT via regulating TLR4/CD14.

necessary for signaling in cancer cells [24, 25]. In addition, immunofluorescence showed that FSTL1 and TLR4/CD14 have extensive co-localization in GC cells (**Figures 7E** and S7). Hence, FSTL1 interacted with TLR4/CD14 in GC. To further verify our hypothesis that TLR4 contributes to optimal activation of AKT by FSTL1, we found that inhibition of TLR4 by TAK-242 (Medchemexpress, USA) reduced the activation of AKT in BGC823 cells overexpressing FSTL1 and abrogated the recFSTL1 induced phosphorylation of AKT (**Figure 7F**, **7G**). Overall, FSTL1 promotes activation of AKT partially dependent on TLR4 signaling.

Discussion

GC, a global threat to human health, represents one of the most malignant tumors. Although a focus of extensive research, detailed mechanisms of GC carcinogenesis and development remain elusive. Therefore, discovery of lurking effective biomarkers that can predict the progression and prognosis of GC to provide clinical significance is urgently needed. In this study, we used a straightforward approach to reveal the expression pattern and clinicopathological features of FSTL1 in GC and its association with prognosis by integrative analysis of multiple cancer databases and clinical samples. Furthermore, functional and mechanism exploration revealed that overexpression of FSTL1 significantly inhibited the apoptosis and promoted metastatic ability of GC cells by triggering AKT-associated signaling pathway via regulating TLR4/CD14. Our results indicated that FSTL1 functions as an oncogene to drive GC and therefore is a promising therapeutic target for the intervention of GC (**Figure 8**).

Identification of proteins with diagnostic and prognostic value may contribute to tumor classification and the development of novel therapies against human cancers. The clinical relevance of FSTL1 has been well reported in various cancers, but it is highly variable with

respect to its expression and prognostic value in different tumors. Compared to normal tissues, reduced expression of FSTL1 was reported in many types of cancers, such as lung adenocarcinoma, ovarian and nasopharyngeal carcinoma.

Low expression of FSTL1 is predictive of poor prognosis in lung adenocarcinoma, endometrial, and ovarian tumors. On the other hand, FSTL1 is higher in breast cancer cells, in most cases of HCC, in cancer-associated-fibroblasts of colon cancer, in ESCC cells than healthy tissues [13, 18, 19, 26-28]. Yang W et al. also suggested that overexpressed FSTL1 in HCC was associated with larger tumors, advanced TNM stages and metastasis [18]. An J reported that FSTL1 was elevated in brain metastatic sites compared to primary breast cancer [13]. Moreover, several studies have reported a correlation between upregulated FSTL1 and poor prognosis in head and neck squamous cell carcinoma in HCC and ESCC patients [18, 19, 29]. In this study, we found that both mRNA and protein expression of FSTL1 was frequently upregulated in GC tissues in TCGA, Oncomine databases and three independent cohorts of 244 GC patients. Furthermore, FSTL1 expression was higher in the stages III and IV samples compared with stages I and II, indicating patients with high FSTL1 in GC are at an increased risk of tumor relapse. Higher FSTL1 was correlated with unfavorable clinical parameters, including the infiltrating depth, unfavorable tumor stage of GC and lymph node metastasis. Besides, patients with a high level of FSTL1 were accompanied by poor survival in K-M plotter, TCGA databases and GC samples. These findings suggested a potentially important role of FSTL1 in the underlying mechanisms of GC.

Considering these findings, it was logical to hypothesize that FSTL1 is involved in the pathogenesis of GC tumorigenicity and/or progression. Previous reports have shown that FSTL1 plays an important role in cancer cell proliferation and malignancy. Yang Y et al. found that FSTL1 not only accelerated breast cancer cell proliferation but also promoted angiogenesis [30]. Sundaram et al. reported that FSTL1 enabled the production of MMP9 by blocking Wnt7a-mediated repression of extracellular signal-regulated kinase phosphorylation toward metastasis [29]. To test this hypothesis, we investigated the role of FSTL1 in the regulation of GC cell proliferation and metastasis using gain- and loss-of function approaches. Our findings indicated that FSTL1 depletion inhibited proliferation by regulating cell apoptosis, migration and invasion of GC cells, while opposite results were observed in GC cells with FSTL1 overexpression in vivo and in vitro. Additionally, upregulated FSTL1 inhibited the expression of apoptosis-associated proteins (BCL2 family) and increased the expression of metastatic proteins (p-FAK, EGFR, snail). These data supported the hypothesis that FSTL1 is an important contributor to GC progression and multiple oncogenic processes.

To investigate the molecular mechanisms of FSTL1 in proliferation and metastasis of GC, we found that FSTL1 may be involved in AKT-associated pathways in GC. The AKT pathway controls basic cellular processes, including cell survival, growth, proliferation, apoptosis, and cell repair, and functions as an oncogene in many types of tumors, including GC [31, 32]. Recent studies reported that FSTL1 activated the AKT pathway in various biological processes, including apoptosis of HCC, and myocardial infarction [18, 33-35]. Yang W et al. reported that FSTL1 repressed cells apoptosis via AKT/GSK-3β pathway in HCC [18]. Liang et al. showed that FSTL1 repressed neuronal apoptosis and improved neurological deficits via FSTL1-DIP2A-AKT pathway [36]. In this study, we showed that FSTL1 regulated the phosphorylation of AKT. At the same time, exogenous FSTL1 enhanced the phosphorylation of AKT and regulated the apoptosis-associated proteins (BCL2 family) and metastasis-correlated proteins (p-FAK, snail, and EGFR). These changes were verified by rescue assays in BGC823 cells. Therefore, FSTL1 promoted the proliferation and metastasis in GC cells via the AKT associated signaling pathway.

Previous studies identified that FSTL1 is a secreted protein that can bind to TLR4, CD14, Follistatin, or DIP2A, which act as membrane receptors [21-23]. Murakami et al. found that FSTL1, interacting with CD14, can evoke an innate immune response via TLR4 signaling. Ouchi et al. showed that DIP2A, as an FSTL1 receptor, regulated the cardiovascular protective roles of FSTL1. In this study, we found that FSTL1 expression positively correlated with the

expression of TLR4 and CD14 in TCGA and GC tissues. Furthermore, FSTL1 in GC regulated TLR4 and CD14, but not DIP2A, and Follistatin. Previous studies showed that TLR4/CD14 (CD14 is a co-Receptor for TLR4) could trigger pro-inflammatory cytokines and contribute to the tumor progression [24, 25]. Meanwhile we found FSTL1 and TLR4, CD14 was extensive co-located in GC cells by Immunofluorescence assays. Based on previous reports and our results, we hypothesized that FSTL1 regulates AKT signaling partially via TLR4/CD14. In the present study, inhibition of TLR4/CD14 in by a TLR4 signaling inhibitor (TAK-242) reduced phosphorylated in FSTL1 overexpressing BGC-823 cells or in response to recFSTL1. Thus, these findings indicated partially dependent on TLR4 signaling. While we were preparing the manuscript, Peng X published their work on FSTL1, and showed that FSTL1 might inhibit GC cell apoptosis via the STAT6 signaling pathway, which also gave evidence for the critical roles of FSTL1 in the development of GC [20].

Conclusions

In summary, this study reports an altered FSTL1 expression pattern in GC and demonstrates its clinical relevance. Furthermore, functional and mechanistic studies suggested a crucial function of FSTL1 in cell proliferation and metastasis through the AKT signaling pathway partially via regulating TLR4/CD14. Therefore, targeting the FSTL1-TLR4/CD14-AKT pathway might be a new therapeutic method to improve the treatment and survival of patients with GC.

Acknowledgements

This work was supported by Project of the regional diagnosis and treatment centre of the Health Planning Committee (JBZX-201903); the Key Research and Development Program of Science and Technology Department of Zhejiang Province (2018C03022); National Health and Family Planning Commission Research Fund & Zhejiang Provincial Medical and Health Major Science and Technology Plan Project (KWJ-ZJ-1802); the National Natural Science Foundation of Zhejiang Province (LQ20H16-0043); Programs for Science and Technology Development of Henan Province (21210231-0198).

Disclosure of conflict of interest

None.

Address correspondence to: Lisong Teng, The First Affiliated Hospital, Zhejiang University School of Medicine, Hangzhou, Zhejiang, P. R. China. Tel: +86-87236878; Fax: +86-87236734; E-mail: lsteng@zju.edu.cn

References

[1] Siegel RL, Miller KD and Jemal A. Cancer statistics, 2018. CA Cancer J Clin 2018; 68: 7-30.
[2] Chen W, Zheng R, Zhang S, Zeng H, Xia C, Zuo T, Yang Z, Zou X and He J. Cancer incidence and mortality in China, 2013. Cancer Lett 2017; 401: 63-71.
[3] Bernards N, Creemers GJ, Nieuwenhuijzen GA, Bosscha K, Pruijt JF and Lemmens VE. No improvement in median survival for patients with metastatic gastric cancer despite increased use of chemotherapy. Ann Oncol 2013; 24: 3056-3060.
[4] Ricciardi MR, Mirabilii S, Licchetta R, Piedimonte M and Tafuri A. Targeting the Akt, GSK-3, Bcl-2 axis in acute myeloid leukemia. Adv Biol Regul 2017; 65: 36-58.
[5] Cory S and Adams JM. The bcl2 family: regulators of the cellular life-or-death switch. Nat Rev Cancer 2002; 2: 647-56.
[6] Datta SR, Dudek H, Tao X, Masters S, Fu H, Gotoh Y and Greenberg ME. Akt phosphorylation of BAD couples survival signals to the cell-intrinsic death machinery. Cell 1997; 91: 231-241.
[7] Kwiatkowska A, Kijewska M, Lipko M, Hibner U and Kaminska B. Downregulation of Akt and FAK phosphorylation reduces invasion of glioblastoma cells by impairment of MT1-MMP shuttling to lamellipodia and downregulates MMPs expression. Biochim Biophys Acta 2011; 1813: 655-67.
[8] Zhou BP, Deng J, Xia W, Xu J, Li YM, Gunduz M and Hung MC. Dual regulation of Snail by GSK-3β-mediated phosphorylation in control of epithelial-mesenchymal transition. Nat Cell Biol 2004; 6: 931-940.
[9] Shibanuma M, Mashimo J, Mita A, Kuroki T and Nose K. Cloning from a mouse osteoblastic cell line of a set of transforming-growth-factor-β1-regulated genes, one of which seems to encode a follistatin-related polypeptide. Eur J Biochem 1993; 217: 13-9.
[10] Peters MMC, Meijs TA, Gathier W, Doevendans PAM, Sluijter JPG, Chamuleau SAJ and Neef K. Follistatin-like 1 in cardiovascular disease and inflammation. Mini Rev Med Chem 2019; 19: 1379-1389.

[11] Mattiotti A, Prakash S, Barnett P and van den Hoff MJB. Follistatin-like 1 in development and human diseases. Cell Mol Life Sci 2018; 75: 2339-2354.
[12] Chaly Y, Hostager B, Smith S and Hirsch R. Follistatin-like protein 1 and its role in inflammation and inflammatory diseases. Immunol Res 2014; 59: 266-272.
[13] An J, Wang L, Zhao Y, Hao Q, Zhang Y, Zhang J, Yang C, Liu L, Wang W, Fang D, Lu T and Gao Y. Effects of FSTL1 on cell proliferation in breast cancer cell line MDAMB231 and its brain metastatic variant MDAMB231BR. Oncol Rep 2017; 38: 3001-3010.
[14] Chan QK, Ngan HY, Ip PP, Liu VW, Xue WC and Cheung AN. Tumor suppressor effect of follistatin-like 1 in ovarian and endometrial carcinogenesis: a differential expression and functional analysis. Carcinogenesis 2009; 30: 114-121.
[15] Bae K, Park KE, Han J, Kim J, Kim K and Yoon KA. Mitotic cell death caused by follistatin-like 1 inhibition is associated with up-regulated Bim by inactivated Erk1/2 in human lung cancer cells. Oncotarget 2016; 7: 18076-18084.
[16] Ni X, Cao X, Wu Y and Wu J. FSTL1 suppresses tumor cell proliferation, invasion and survival in non-small cell lung cancer. J Cell Physiol 2018; 39: 13-20.
[17] Zhou X, Xiao X, Huang T, Du C, Wang S, Mo Y, Ma N, Murata M, Li B, Wen W, Huang G, Zeng X and Zhang Z. Epigenetic inactivation of follistatin-like 1 mediates tumor immune evasion in nasopharyngeal carcinoma. Oncotarget 2016; 7: 16433-16444.
[18] Yang W, Wu Y, Wang C, Liu Z, Xu M and Zheng X. FSTL1 contributes to tumor progression via attenuating apoptosis in a AKT/GSK-3beta -dependent manner in hepatocellular carcinoma. Cancer Biomark 2017; 20: 75-85.
[19] Lau MC, Ng KY, Wong TL, Tong M, Lee TK, Ming XY, Law S, Lee NP, Cheung AL, Qin YR, Chan KW, Ning W, Guan XY and Ma S. FSTL1 promotes metastasis and chemoresistance in esophageal squamous cell carcinoma through NFkappaB-BMP signaling cross-talk. Cancer Res 2017; 77: 5886-5899.
[20] Peng X, Wang P, Li S, Jiang Y and Wu C. Follistatin-like protein 1 knockdown elicits human gastric cancer cell apoptosis via a STAT6-dependent pathway. Oncol Rep 2019; 42: 2806-2813.
[21] Murakami K, Tanaka M, Usui T, Kawabata D, Shiomi A, Iguchi-Hashimoto M, Shimizu M, Yukawa N, Yoshifuji H, Nojima T, Ohmura K, Fujii T, Umehara H and Mimori T. Follistatin-related protein/follistatin-like 1 evokes an innate immune response via CD14 and toll-like receptor 4. FEBS Lett 2012; 586: 319-324.
[22] Ouchi N, Asaumi Y, Ohashi K, Higuchi A, Sono-Romanelli S, Oshima Y and Walsh K. DIP2A functions as a FSTL1 receptor. J Biol Chem 2010; 285: 7127-7134.
[23] Geng Y, Dong Y, Yu M, Zhang L, Yan X, Sun J, Qiao L, Geng H, Nakajima M, Furuichi T, Ikegawa S, Gao X, Chen YG, Jiang D and Ning W. Follistatin-like 1 (Fstl1) is a bone morphogenetic protein (BMP) 4 signaling antagonist in controlling mouse lung development. Proc Natl Acad Sci U S A 2011; 108: 7058-7063.
[24] He Z, Riva M, Björk P, Swärd K, Mörgelin M, Leanderson T and Ivars F. CD14 is a co-receptor for TLR4 in the S100A9-induced pro-inflammatory response in monocytes. PLoS One 2016; 11: e0156377.
[25] Płóciennikowska A, Hromada-Judycka A, Borzęcka K and Kwiatkowska K. Co-operation of TLR4 and raft proteins in LPS-induced pro-inflammatory signaling. Cell Mol Life Sci 2015; 72: 557-581.
[26] Cheng S, Huang Y, Lou C, He Y, Zhang Y and Zhang Q. FSTL1 enhances chemoresistance and maintains stemness in breast cancer cells via integrin beta3/Wnt signaling under miR-137 regulation. Cancer Biol Ther 2019; 20: 328-337.
[27] Bevivino G, Sedda S, Franze E, Stolfi C, Di Grazia A, Dinallo V, Caprioli F, Facciotti F, Colantoni A, Ortenzi A, Rossi P and Monteleone G. Follistatin-like protein 1 sustains colon cancer cell growth and survival. Oncotarget 2018; 9: 31278-31290.
[28] Su S, Parris AB, Grossman G, Mohler JL, Wang Z and Wilson EM. Up-regulation of follistatin-like 1 by the androgen receptor and melanoma antigen-A11 in prostate cancer. Prostate 2017; 77: 505-516.
[29] Sundaram GM, Ismail HM, Bashir M, Muhuri M, Vaz C, Nama S, Ow GS, Vladimirovna IA, Ramalingam R, Burke B, Tanavde V, Kuznetsov V, Lane EB and Sampath P. EGF hijacks miR-198/FSTL1 wound-healing switch and steers a two-pronged pathway toward metastasis. J Exp Med 2017; 214: 2889-2900.
[30] Yang Y, Mu T, Li T, Xie S, Zhou J and Liu M. Effects of FSTL1 on the proliferation and motility of breast cancer cells and vascular endothelial cells. Thorac Cancer 2017; 8: 606-612.
[31] Vanhaesebroeck B, Stephens L and Hawkins P. PI3K signalling: the path to discovery and understanding. Nat Rev Mol Cell Biol 2012; 13: 195-203.
[32] Martini M, De Santis MC, Braccini L, Gulluni F and Hirsch E. PI3K/AKT signaling pathway and cancer: an updated review. Ann Med 2014; 46: 372-383.
[33] Oshima Y, Ouchi N, Sato K, Izumiya Y, Pimentel DR and Walsh K. Follistatin-like 1 is an Akt-

regulated cardioprotective factor that is secreted by the heart. Circulation 2008; 117: 3099-3108.
[34] Altekoester AK and Harvey RP. Bioengineered FSTL1 patches restore cardiac function following myocardial infarction. Trends Mol Med 2015; 21: 731-733.
[35] Chiba A, Watanabe-Takano H, Miyazaki T and Mochizuki N. Cardiomyokines from the heart. Cell Mol Life Sci 2018; 75: 1349-1362.
[36] Liang X, Hu Q, Li B, McBride D, Bian H, Spagnoli P, Chen D, Tang J and Zhang JH. Follistatin-like 1 attenuates apoptosis via disco-interacting protein 2 homolog A/Akt pathway after middle cerebral artery occlusion in rats. Stroke 2014; 45: 3048-3054.

Supplementary Methods

Quantitative real-time PCR (qRT-PCR)

Total RNA was extracted from the tissue samples and cells using TRIzol reagent (Invitrogen, Carlsbad, California, USA) according to the manufacturer's instructions. One microgram RNA per sample was reverse transcribed to cDNA using the PrimeScript RT reagent kit (Takara, Kyoto, Japan), and amplified by qRT-PCR using SYBR Green reaction system (Takara, Kyoto, Japan). Relative expression of FSTL1 was calculated by the 2-ΔΔCt method, with GAPDH as the internal control. All primer sequences were as followings: FSTL1, forward: 5'-GAGCAATGCAAACCTCACAAG-3' and reverse: 5'-CAGTGTCCATCGTAATCAACCTG-3'; TLR4, forward: 5'-AGACCTGTCCCTGAACCCTAT-3' and reverse: 5'-CGATGGACTTCTAAACCAGCCA-3'; CD14, forward: 5'-GACCTAAAGATAACCGGCACC-3' and reverse: 5'-GCAATGCTCAGTACCTTGAGG-3'; GAPDH, forward: 5'-GGAGCGAGATCCCTCCAAAAT-3' and reverse: 5'-GGCTGTTGTCATACTTCTCATGG-3'.

Immunohistochemistry (IHC)

Paraffin-embedded GC sections were deparaffinized in xylene, dehydrated through an ethanol gradient, and blocked with 3% H_2O_2 for 10 min. The slides were then heated in citrate buffer (pH 6) at 95°C for 15-20 min for antigen retrieval. The tissue sections were incubated overnight with anti-FSTL1 antibody (1:200 diluted, Proteintech, USA), or anti-ki67 antibody (1:200 diluted, Proteintech, USA) at 4°C, followed by a 30 min incubation with HRP-conjugated secondary antibody (ZSGB-bio, Beijing, China) at 37°C. After washing three times with PBS, color was developed using DAB Chromogen (ZSGB-bio, Beijing, China). Slides were then rinsed in tap water and counterstained with hematoxylin. Five random fields per section were viewed under a light microscope, and FSTL1 expression was scored for intensity of staining and percentage of positive-stained area. The positive rate was scored on a scale from 0 to 5 (0 - no staining, 1- ≤ 20%, 2- ≤ 40%, 3- ≤ 60%, 4- ≤ 80%, and 5- > 80%), and the staining intensity was graded as 0 (negative), 1 (weak), 2 (moderate) or 3 (strong).

Cell proliferation assay

Cell viability and proliferation was assessed using CCK-8 assay, and colony formation assay. For CCK-8 assay, cells were seeded in 96-well plates. After cell growth, culture medium was removed and 10 μl CCK8 in 100 μl culture medium was added to each well, followed by 2 hours incubation. Absorbance was measured at 450 nm for proliferation.

For colony formation assay, GC cells were seeded in 6-well plates, and incubated at 37°C for 10 days. Colonies containing at least 50 cells were scored.

Cell apoptosis assay

Cells treated for 48 hours were harvested, washed twice by PBS, and stained with FITC-AnnexinV and PI. Cell cycle and apoptosis were analyzed by flow cytometry (BD FACS Calibur, Becton Dickinson, San Jose, CA, USA).

Cell migration and invasion assay

Cell migration and invasion assay were performed in Transwell chambers (24-well format, 8.0 um pore size, Millipore, Washington, DC, USA). 3×10^4 cells in serum-free media were seeded in uncoated upper chamber for migration assay, and 8×10^4 cells in serum-free media were cultured in Matrigel (BD Biosciences, Lake Franklin, NJ, USA)-coated chamber for cell invasion assays. Culture medium with 10% FBS was added in the lower chamber. After 24 hours of incubation, cells that had moved from the upper surface of membrane to the lower side were washed twice by PBS, fixed in 4% paraformaldehyde and stained in Giemsa. Number of migrated cells was counted in five random fields (200 ×) under a light microscope.

Western blot

Total proteins from tissues or cells were extracted with RIPA lysis buffer (Beyotime Inc., China), containing with phenylmethanesulfonyl fluoride (Beyotime Inc., China) and protease inhibitor cocktail (Beyotime Inc., China). 20 μg protein per sample was separated by SDS-PAGE and transferred to a PVDF membrane (Millipore Inc., USA). Membranes were incubated with primary antibody at 4°C overnight followed by an HRP-conjugated secondary antibody (Cell Signaling Technology, USA). Anti-GAPDH antibody (Cell Signaling Technology, USA) was used as an internal control. Protein bands were detected with ECL chromogenic substrate (Beyotime Inc., China) and the relative protein expression was quantified by Image J. The primary antibodies are as following: FSTL1 (1 ug/ml, AF1694, R&D); TLR4 (1:1000, ab13556, Abcam); CD14 (1:1000, ab181470, Abcam); Mcl1 (1:1000, ab32087, Abcam); Bcl2 (1:1000, ab182858, Abcam); Bcl-xl (1:1000, 2764S, CST); Bim (1:1000, 2933T, CST); Bax (1:1000, 5023S, CST); EGFR (1:1000, ab52894, Abcam); p-FAK (1:500, ab76120, Abcam); FAK (1:1000, ab40794, Abcam); Snail (1:100, 3879S, CST); p-AKT (1:1000, 9271S, CST); AKT (1:1000, 9272S, CST); Follistain (1:500, ab157471, Abcam) and DIP2A (1:150, sc-293390, Santa sruz).

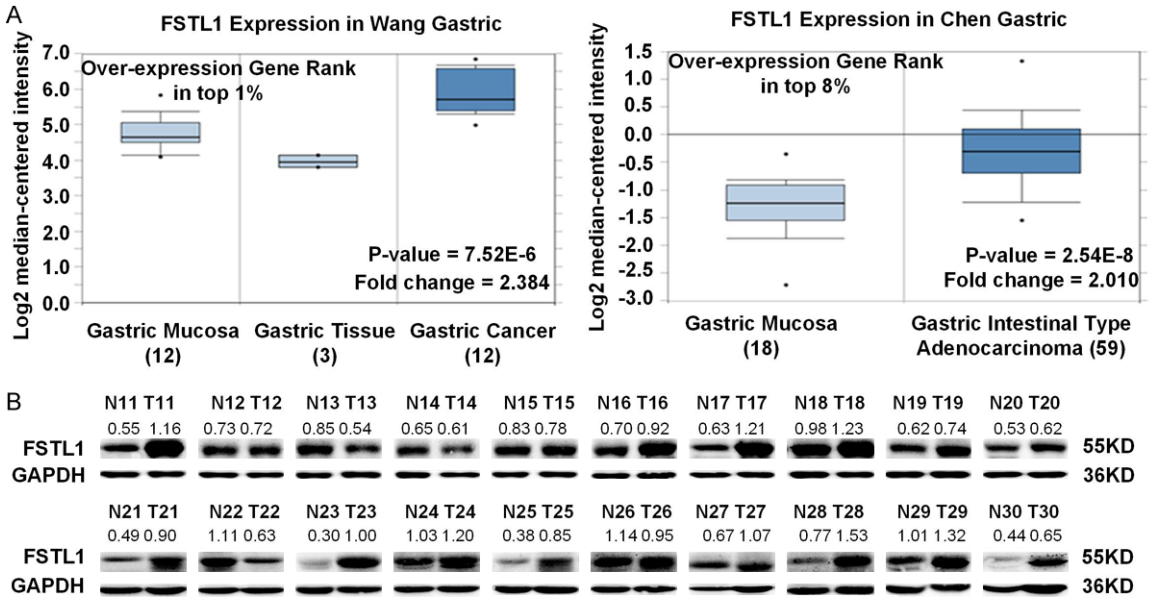

Figure S1. The expression level of FSTL1 in GC. A. FSTL1 mRNA levels in GC and normal gastric tissue in Oncomine database. Shown are fold changes, associated *p* values, and overexpression gene rank, based on Oncomine 4.5 analysis. B. Representative images of FSTL1 proteins level in Zhejiang cohort 2 (Sample 11-30).

Table S1. Association between FSTL1 expression and clinicopathological features of GC in TCGA database

	No. patients	High expression (n = 191)	Low expression (n = 190)	*P* value
Gender				
male	245 (64.3%)	121 (31.8%)	124 (32.5%)	0.6969[a]
female	136 (35.7%)	70 (18.4%)	66 (17.3%)	
Age				
≤ 60	124 (32.5%)	67 (17.6%)	57 (15.0%)	0.2901[a]
> 60	257 (67.5%)	124 (32.5%)	133 (34.9%)	
T stage				
T1	19 (5.0%)	3 (0.8%)	16 (4.2%)	0.0011[b]
T2	79 (20.7%)	34 (8.9%)	45 (11.8%)	
T3	173 (45.4%)	91 (23.9%)	82 (21.5%)	
T4	110 (28.9%)	63 (16.5%)	47 (12.3%)	
N stage				
N0	119 (31.2%)	57 (15.0%)	62 (16.3%)	0.2294[b]
N1	100 (26.2%)	48 (12.6%)	52 (13.6%)	
N2	76 (19.9%)	38 (10.0%)	38 (10.0%)	
N3	81 (21.3%)	46 (12.1%)	35 (9.2%)	
NX	5 (1.3%)			
M stage				
M0	340 (89.2%)	168 (44.1%)	172 (45.1%)	0.3246[b]
M1	27 (7.1%)	16 (44.1%)	11 (2.9%)	
MX	14 (3.7%)			
AJCC stage				
I	54 (14.2%)	18 (4.7%)	36 (9.4%)	0.0252[b]
II	120 (31.5%)	62 (16.3%)	58 (15.2%)	
III	166 (43.6%)	88 (23.1%)	78 (20.5%)	
IV	39 (10.2%)	22 (5.8%)	17 (4.5%)	
Missing	2 (0.5%)			

a: chi-square test; b: Yates' continuity corrected chi-square test.

Table S2. Association between FSTL1 expression and clinicopathological features of GC in Zhejiang cohort 1

	No. patients	Low expression (n = 54)	High expression (n = 54)	*P* value
Gender				
Male	84 (77.8%)	45 (41.7%)	39 (36.1%)	0.1649
Female	24 (22.2%)	9 (8.3%)	15 (13.9%)	
Age				
≤ 60	40 (37.0%)	20 (18.5%)	20 (18.5%)	1.0000
> 60	68 (63.0%)	34 (31.5%)	34 (31.5%)	
Grade				
G1-2	87 (80.6%)	42 (38.9%)	45 (41.7%)	0.4658
G3	21 (19.4%)	12 (11.1%)	9 (8.3%)	
T stage				
T1-2	31 (28.7%)	23 (21.3%)	8 (7.4%)	0.0014*
T3-4	77 (71.3%)	31 (28.7%)	46 (42.6%)	
N stage				
N0	27 (25.0%)	21 (19.4%)	6 (5.6%)	0.0009*
N1-3	81 (75%)	33 (30.6%)	48 (44.4%)	
M stage				
M0	90 (83.3%)	46 (43.6%)	44 (40.7%)	0.6056
M1	18 (16.7%)	8 (7.4%)	10 (9.3%)	
Tumor size				
≤ 5 cm	62 (57.4%)	33 (30.6%)	29 (26.8%)	0.4363
> 5 cm	46 (42.6%)	21 (19.4%)	25 (23.2%)	
AJCC stage				
I-II	36 (33.3%)	25 (23.1%)	11 (10.2%)	0.0043*
III-IV	72 (66.7%)	29 (26.9%)	43 (39.8%)	

*chi-square test.

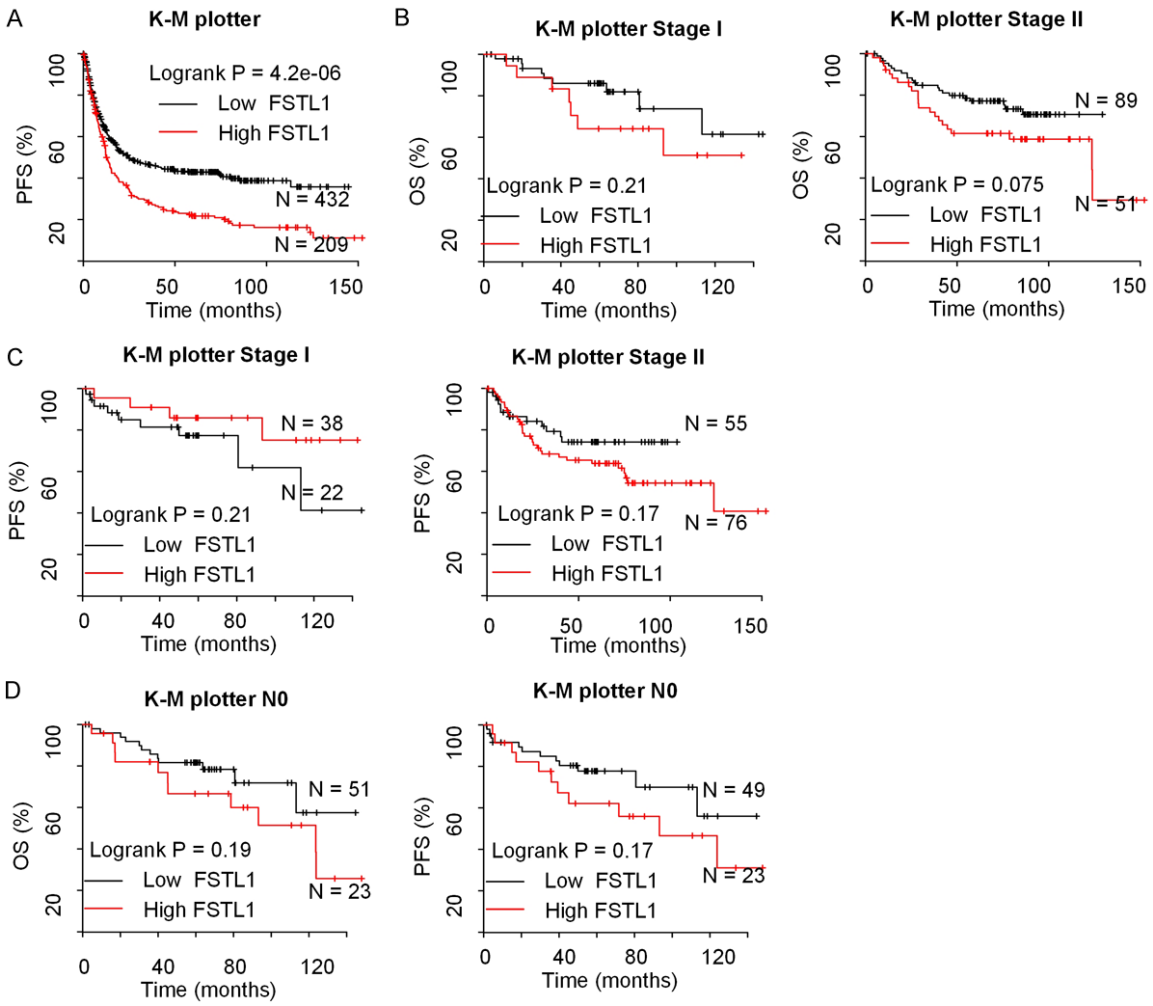

Figure S2. FSTL1 is associated with poor prognosis in GC. A. Kaplan-Meier curves for PFS of GC patients using K-M plotter database. B, C. Kaplan-Meier curves for OS and PFS of GC patients with stage I/II using K-M plotter database. D. OS and PFS for GC patients with N0 disease.

Table S3. Correlation of FSTL1 mRNA expression and clinical prognosis in GC with different clinico-pathological factors by K-M plotter

	Overal Survival (n = 882)			Progression-free Survival (n = 646)		
	N	Hazard Rate	*P*-Value	N	Hazard Rate	*P*-Value
Sex						
Female	236	1.89 (1.33-2.70)	0.00035	201	1.97 (1.35-2.87)	0.00036
Male	545	1.62 (1.31-2.01)	7.9e-06	438	1.60 (1.26-2.03)	9.2e-05
Stage						
1	67	1.87 (0.69-5.07)	0.21	60	0.47 (0.14-1.57)	0.21
2	140	1.71 (0.94-3.12)	0.075	131	1.60 (0.82-3.12)	0.17
3	305	1.75 (1.31-2.34)	0.00012	186	1.94 (1.34-2.81)	0.00036
4	148	1.89 (1.28-2.81)	0.0013	141	1.58 (1.05-2.37)	0.026
Stage T						
2	241	2.14 (1.40-3.27)	3e-04	239	1.85 (1.23-2.80)	0.0029
3	204	1.72 (1.21-2.45)	0.0022	204	1.60 (1.14-2.26)	0.0063
4	38	3.17 (1.30-7.71)	0.0074	39	4.67 (1.87-11.66)	0.00035
Stage N						
0	74	1.75 (0.76-4.06)	0.19	72	1.78 (0.78-4.08)	0.17
1	223	2.34 (1.55-3.53)	3.1e-05	222	2.35 (1.59-3.48)	9.1e-06
2	121	1.91 (1.22-2.99)	0.0043	125	2.06 (1.33-3.18)	0.00088
3	76	2.40 (1.40-4.12)	0.0011	76	1.96 (1.15-3.34)	0.012
1+2+3	422	2.15 (1.66-2.80)	5e-09	423	2.19 (1.70-2.82)	5.4e-10
Stage M						
0	444	2.04 (1.55-2.70)	2.9e-07	443	2.08 (1.59-2.71)	3.3e-08
1	56	2.05 (1.12-3.75)	0.018	56	1.57 (0.85-2.89)	0.14
Lauren classification						
Diffuse	241	2.05 (1.45-2.89)	3.5e-05	231	2.07 (1.46-2.93)	2.6e-05
Intestinal	320	2.32 (1.69-3.19)	1e-07	263	2.01 (1.39-2.89)	0.00014
Mixed	32	2.29 (0.82-6.35)	0.1	28	2.71 (0.76-9.64)	0.11
Differentiation						
Poorly	165	1.37 (0.92-2.05)	0.12	121	1.42 (0.90-2.25)	0.13
Moderately	67	1.95 (0.99-3.86)	0.051	67	2,32 (1.19-4.52)	0.011
Well	32	13.34 (3.03-58.81)	1.8e-05	/	/	/
HER2 status						
Positive	344	1.67 (1.27-2.19)	0.00019	233	1.75 (1.20-2.55)	0.0034
Negative	532	1.63 (1.30-2.04)	1.7e-05	408	1.75 (1.35-2.27)	1.5e-05
Treatment						
Surgery alone	380	1.77 (1.32-2.37)	0.00011	375	1.76 (1.33-2.33)	6.7e-05
5-FU based adjuvant	153	0.80 (0.56-1.15)	0.23	153	0.86 (0.61-1.21)	0.38
Other adjuvant	76	3.37 (1.40-8.10)	0.004	80	3.95 (1.65-9.46)	9e-04

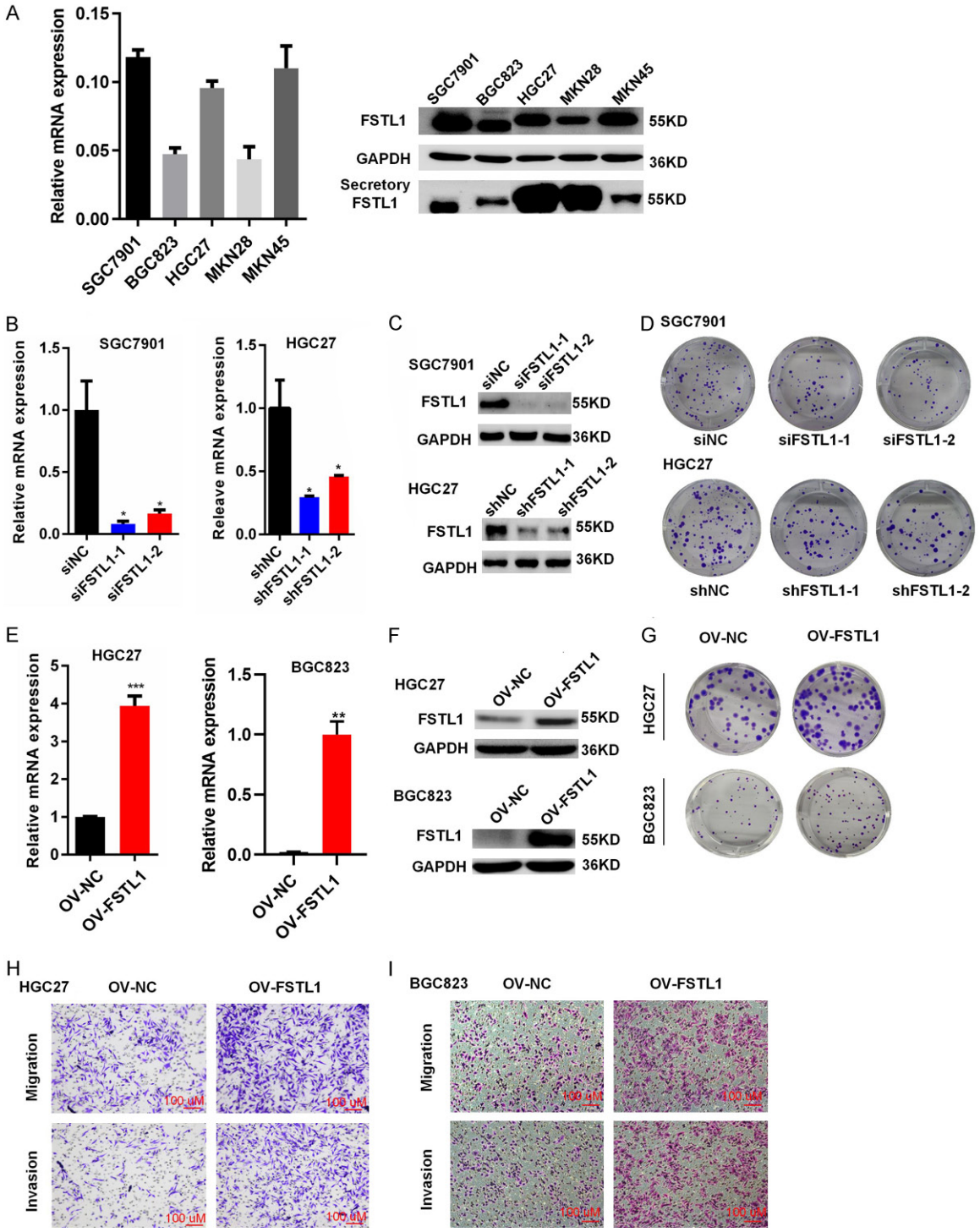

Figure S3. The role of FSTL1 in GC. A. The mRNA, endogenous and secretory protein expression levels of FSTL1 were checked in a panel of five human GC cell lines using RT-qPCR and western blot. B, C. mRNA and protein expression level of FSTL1 were efficiently inhibited by siFSTL1/siNC or shFSTL1/NC in SGC7901 and HGC27 cells. D. Representative images of colony formation assay in SGC7901 and HGC27 cells transfected with siRNA/NC or shRNA/NC. E, F. mRNA and protein expression level of FSTL1 were efficiently upregulated in HGC27 and BGC823 cells transfected with OV-FSTL1/NC. G. Representative images of colony formation assay in HGC27 and BGC823 cells transfected with OV-FSTL1/NC. H, I. Representative images of migration and invasion assay in HGC27 and BGC823 cells transfected with OV-FSTL1/NC (SP, × 200).

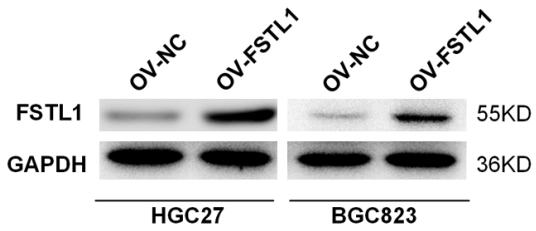

Figure S4. The FSTL1 level was stably elevated in HGC27 and BGC823 cells transfected with lentivitus vector OV-FSTL1/NC.

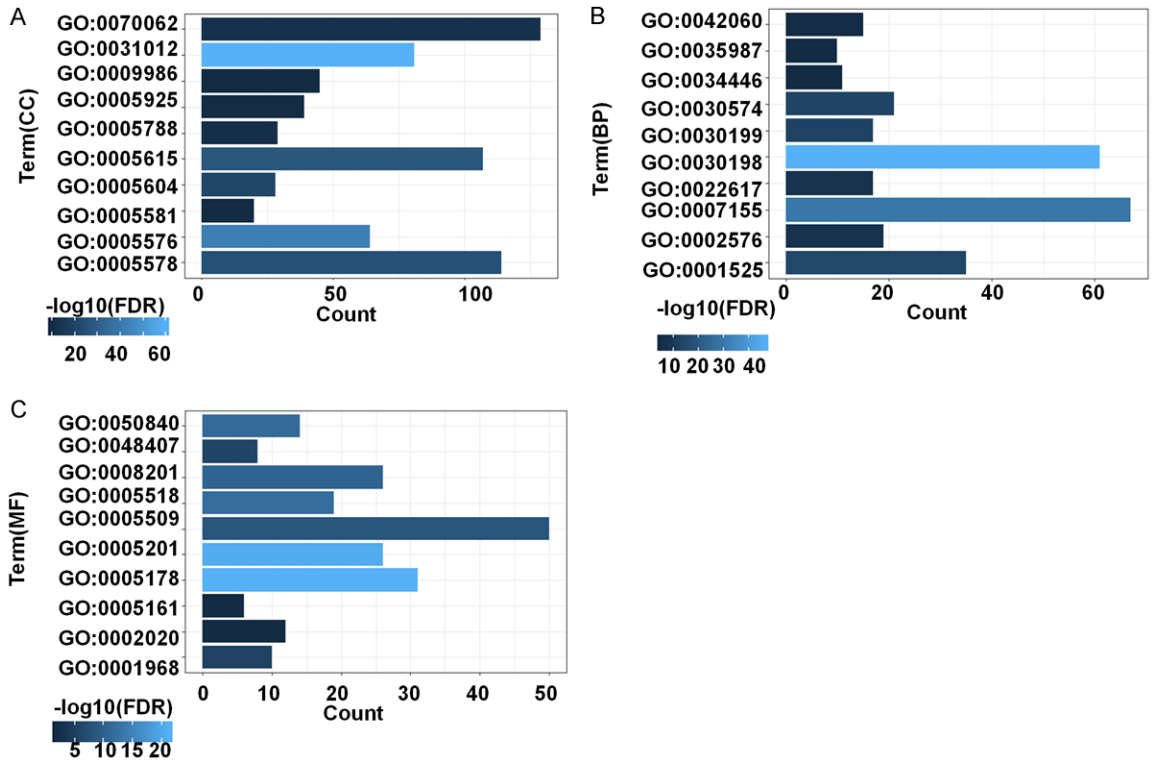

Figure S5. GO analysis of MAGP1 co-expressed genes in GC. A. Cellular components (CCs); B. Biological processes (BPs); C. Molecular factors (MFs). GO, gene ontology.

Table S5. GO analysis of FSTL1 co-expressed genes in GC

Category	GO ID	Number of genes	Associated Genes (%)	Term *P* Value	Term FDR	Associated Genes Found
MF	GO:0005178	31	7.451923	2.50522E-25	3.57E-22	TSPAN4, COL3A1, TIMP2, ITGB1, VCAM1, S1PR3, WISP1, LAMB2, CTGF, FAP, TGFBI, THBS1, FN1, CYR61, TNXB, FBN1, ACTN1, IGF1, MFGE8, ECM2, MMP14, COL16A1, COL5A1, THY1, VWF, FBLN1, SFRP2, ITGA5, FBLN5, JAM3, ADAMTS5
MF	GO:0005201	26	6.25	1.34851E-24	1.92E-21	PXDN, LUM, COL3A1, ELN, LAMB1, COL8A2, COL4A2, COL4A1, TNXB, EFEMP2, FBN1, COL15A1, MGP, COL5A2, COL5A1, PRELP, FBLN1, LAMA4, BGN, COL14A1, FBLN2, COL1A2, VCAN, COL1A1, LAMC1, MFAP5
MF	GO:0005518	19	4.567308	4.15366E-16	6.33E-13	SPARCL1, LUM, MRC2, ITGA11, NID1, SPARC, DCN, NID2, DDR2, ABI3BP, PCOLCE, P3H1, VWF, CTSK, COL14A1, C1QTNF1, TGFBI, ANTXR1, FN1
MF	GO:0050840	14	3.365385	1.97895E-15	2.84E-12	SPARCL1, OLFML2B, CD248, ELN, ITGB3, SPARC, DCN, BGN, FBLN2, ITGAV, TGFBI, THBS1, ADAMTS5, CYR61
MF	GO:0008201	26	6.25	1.44278E-14	2.05E-11	NRP1, LTBP2, POSTN, ABI3BP, PCOLCE, OGN, WISP1, SERPINE2, CTGF, CRISPLD2, CFH, THBS1, THBS2, FN1, CYR61, TNXB, FBN1, CCDC80, ECM2, COL5A1, SLIT2, PRELP, SLIT3, CLEC3B, ADAMTS1, ADAMTS5
MF	GO:0005509	50	12.01923	2.00354E-12	2.85E-09	PAM, FKBP7, LTBP2, CD248, SPOCK1, C1S, MYL9, ANXA6, HMCN1, CD93, SLC24A3, PKD2, HEG1, THBS1, THBS2, EHD2, BMP1, SVEP1, SPARCL1, EFEMP2, EFEMP1, FBN1, MMP19, HSPG2, MGP, ACTN1, NID1, NID2, SPARC, PCDH17, MMP14, SLIT2, SLIT3, PCDH18, NOTCH3, NOTCH2, FBLN1, EML1, LRP1, THBD, PLSCR4, CLEC3B, FBLN2, FBLN5, SULF1, FKBP14, VCAN, RCN3, ADGRL4, CDH11
MF	GO:0048407	8	1.923077	7.57661E-10	1.08E-06	COL4A1, COL3A1, PDGFRA, COL1A2, PDGFRB, COL6A1, COL1A1, COL5A1
MF	GO:0001968	10	2.403846	2.61734E-09	3.72E-06	CTSK, FBLN1, SFRP2, CTGF, ITGAV, CCDC80, ITGB3, THBS1, ITGB1, IGFBP5
MF	GO:0005161	6	1.442308	1.29967E-05	0.018495	IL1R1, ITGA5, PDGFRA, PDGFRB, PDGFC, ITGB3
MF	GO:0002020	12	2.884615	1.45607E-05	0.02072	VWF, IL1R1, A2M, LRP1, ITGAV, FAP, ITGB3, TIMP2, TIMP3, ITGB1, FN1, TIMP1
CC	GO:0031012	81	19.47115	4.54398E-64	6.11E-61	AEBP1, RARRES2, PXDN, LTBP2, IGFBP7, TGFB3, POSTN, MMP2, MMRN2, OGN, HMCN1, SERPINE2, CD93, HTRA1, TGFBI, COL12A1, LOXL2, LOXL1, SPON1, CYR61, MMP19, CILP, MGP, MFGE8, MMP14, FLNA, PRELP, BGN, SERPINF1, COL1A2, VCAN, LAMC1, TGFB1I1, COL1A1, MFAP4, TNC, LUM, VIM, COL3A1, DCN, TIMP2, TIMP3, PCOLCE, ABI3BP, LAMB2, COL6A3, COL6A2, COL6A1, ADAMTS12, COL8A1, LAMB1, THBS1, THBS2, COL8A2, DPT, FN1, COL18A1, PLAT, COL4A2, TNXB, COL4A1, LGALS1, FBN1, EFEMP1, LMCD1, COL15A1, HSPG2, NID1, NID2, COL5A2, COL5A1, EMILIN1, LAMA2, VWF, FBLN1, LAMA4, COL14A1, CLEC3B, FBLN2, SFRP2, FBLN5
CC	GO:0005578	64	15.38462	3.56721E-46	4.79E-43	CTHRC1, PXDN, LTBP2, POSTN, MMP2, OGN, WISP1, CTGF, GPC6, TGFBI, LOX, SPON2, SPON1, CYR61, SPARCL1, OLFML2B, MMP19, CILP, MGP, SLIT2, PRELP, SLIT3, BGN, COL1A2, VCAN, ADAMTS1, ADAMTS2, ADAMTS5, MAMDC2, CD248, LUM, ELN, SPOCK1, TIMP2, TIMP3, TIMP1, P3H1, CRISPLD2, COL6A3, COL6A2, ADAMTS12, COL8A2, DPT, FN1, COL18A1, FLRT2, TNXB, BMP1, LGALS1, FBN1, EFEMP1, COL15A1, SPARC, COL16A1, ECM2, COL5A2, COL5A1, EMILIN1, VWF, FBLN1, OMD, COL14A1, FBLN2, FBLN5
CC	GO:0005615	107	25.72115	2.20258E-31	2.96E-28	CTHRC1, LTBP2, TGFB3, POSTN, MMP2, CXCL12, MMRN2, OGN, PTGIS, SERPINE2, HTRA1, CTGF, FAP, TGFBI, CFH, COL12A1, PDGFC, LOX, CFD, SPON2, SPON1, SPARCL1, ACTN1, SERPING1, MFGE8, PRELP, THBD, SERPINF1, COL1A2, LAMC1, COL1A1, ADAMTS5, PAM, TIMP2, GREM1, TIMP3, ABI3BP, TIMP1, LAMB1, ANGPTL2, FN1, COL18A1, PLAT, BMP1, LGALS1, EFEMP1, LMCD1, ECM2, OMD, COL14A1, SRPX2, SFRP2, SFRP4, PXDN, AEBP1, NRP1, IGFBP7, LRRC17, WISP1, GPC6, SEMA3C, MSN, LOXL2, LOXL1, ACTA2, CILP, SLIT2, SLIT3, CTSK, PLXDC1, CTSO, VCAN, JAM3, C3, TNC, LUM, CPQ, COL3A1, SPOCK1, DCN, PCOLCE, VCAM1, C1QTNF1, COL6A3, COL6A2, THBS1, DPT, FLRT2, TNXB, FBN1, COL15A1, AXL, HSPG2, IGF1, DPYSL3, SPARC, CLEC11A, SH3BGRL, DKK3, FBLN1, CLEC3B, FBLN5, PECAM1, SULF1, C1RL, CMTM3, IGFBP4
CC	GO:0005576	114	27.40385	3.76939E-29	5.06E-26	A2M, RARRES2, F13A1, TGFB3, MMP2, CXCL12, OLFML1, OGN, SERPINE2, HTRA1, CTGF, TGFBI, CFH, COL12A1, PDGFC, LOX, HTRA3, CFD, OLFML2B, ACTN1, SERPING1, MFGE8, PRELP, SERPINF1, PDGFRL, COL1A2, LAMC1, COL1A1, MFAP4, MFAP5, ADAMTS2, ADAMTS5, IL1R1, ELN, TIMP2, TIMP3, TIMP1, FAM19A5, ITGBL1, LAMB2, HEG1, LAMB1, FN1, COL18A1, PLAT, BMP1, EFEMP2, EFEMP1, COL16A1, EPHA3, EMILIN1, NOTCH3, LAMA2, NOTCH2, OMD, LAMA4, COL14A1, SFRP2, SFRP4, IGFBP7, LEPR, LOXL1, CYR61, MMP19, SLIT2, FLNA, SLIT3, CTSK, BGN, PLXDC1, VCAN, CHSY1, ADAM12, C3, TNC, LUM, COL3A1, C1S, DCN, ISLR, CRISPLD2, GLIPR1, C1QTNF1, FNDC1, COL6A3, COL6A2, COL6A1, COL8A1, THBS1, FIBIN, COL8A2, THBS2, COL4A2, COL4A1, SVEP1, FBN1, COL15A1, HSPG2, IGF1, NID1, NID2, SPARC, COL5A2, COL5A1, CLEC11A, VWF, DKK3, FBLN1, CLEC3B, FBLN2, FBLN5, IGFBP4, F2R, IGFBP5

CC	GO:0005604	28	6.730769	4.60262E-25	6.18E-22	TNC, TIMP3, MMRN2, TIMP1, HMCN1, LAMB2, TGFBI, LOXL2, LAMB1, COL8A2, LOXL1, THBS2, COL18A1, COL4A1, EFEMP2, FBN1, HSPG2, CCDC80, NID1, NID2, SPARC, COL5A1, LAMA2, LAMA4, FBLN1, SERPINF1, ADAMTS1, LAMC1
CC	GO:0070062	129	31.00962	3.43158E-16	4.44E-13	RARRES2, A2M, LTBP2, CXCL12, MMRN2, PRKAR2B, OGN, DAB2, HMCN1, HTRA1, PLOD2, TGFBI, CFH, COL12A1, PDGFC, CFD, SPON2, CRYAB, SPARCL1, ACTN1, MGP, SERPING1, MRGPRF, COLEC12, MFGE8, PRELP, THY1, SERPINF1, COL1A2, PDGFRB, LAMC1, MFAP4, PAM, ITGB3, TIMP2, TIMP3, ITGB1, TIMP1, P3H1, LAMB2, ITGAV, ENTPD1, LAMB1, ANGPTL2, FN1, COL18A1, PLAT, BHMT2, CACNA2D1, EFEMP2, LGALS1, EFEMP1, EMILIN1, LAMA2, OMD, LAMA4, COL14A1, ANTXR1, DNAJB4, MYLK, RHOJ, CYB5R3, PXDN, AEBP1, IGFBP7, GJA1, RHOQ, DDR2, SEMA3C, TUBB6, MSN, FAM129A, TUBA1A, AHNAK, CLMP, ACTA2, CILP, WLS, SLIT2, FLNA, BGN, CLIC4, PLXDC2, CYBRD1, GNB4, C3, LUM, CD248, CPQ, VIM, C1S, PCOLCE, VCAM1, ANXA6, ISLR, CRISPLD2, COL6A3, PKD2, COL6A2, COL6A1, COL8A1, THBS1, EHD2, DPT, FLRT2, COL4A2, TNXB, FBN1, HSPG2, COL15A1, AXL, NID1, MXRA8, NID2, DPYSL2, FZD4, COL5A1, VWF, SH3BGRL, FBLN1, PLSCR4, CLEC3B, FBLN2, FBLN5, PECAM1, C1RL, FCGR2A, PRSS23, CDH11
CC	GO:0005788	29	6.971154	3.53774E-15	4.77E-12	FKBP7, COL3A1, P3H1, KDELC1, FMO1, P4HA3, COL6A3, COL6A2, COL6A1, COL12A1, GPX8, PDGFC, COL8A1, THBS1, COL8A2, SPON1, COL18A1, COL4A2, COL4A1, COL15A1, COL16A1, COL5A2, COL5A1, COL14A1, COL1A2, FKBP14, COL1A1, RCN3, ADAMTS5
CC	GO:0005925	39	9.375	3.15178E-14	4.24E-11	DLC1, NRP1, CNN3, FHL1, TNC, TSPAN4, VIM, PEAK1, FERMT2, ITGA11, AKAP12, GJA1, ITGB3, DDR2, ITGB1, ANXA6, DAB2, FAP, ITGAV, MSN, AHNAK, NOX4, FLRT2, MRC2, HSPG2, ACTN1, CSRP2, NEXN, MMP14, PALLD, FLNA, THY1, LRP1, TNS1, LAYN, ITGA5, PDGFRB, TGFB1I1, PARVA
CC	GO:0005581	20	4.807692	1.64727E-13	2.21E-10	COL18A1, CTHRC1, COL3A1, COL15A1, COLEC12, COL5A2, COL5A1, PCOLCE, TIMP1, EMILIN1, COL14A1, C1QTNF1, COL6A3, COL1A2, COL6A2, COL12A1, COL6A1, COL1A1, LOX, COL8A2
CC	GO:0009986	45	10.81731	1.67392E-13	2.25E-10	PAM, IL1R1, NRP1, ACVRL1, ADGRF5, FERMT2, TGFB3, ITGB3, LPAR1, GREM1, TIMP2, ITGB1, SDC2, VCAM1, SRPX, CD93, ITGAV, FAP, PDGFC, THBS1, CSF1R, PLAT, CLMP, CRYAB, LGALS1, AXL, MXRA8, SPARC, FZD4, SLIT2, NOTCH2, TNS1, THBD, BGN, SRPX2, LAYN, ITGA5, CLIC4, SFRP4, SULF1, PDGFRB, ANTXR1, ADGRA2, SCARA5, F2R
BP	GO:0030198	61	14.66346	1.08037E-50	1.85E-47	PXDN, POSTN, DDR2, FOXF1, TGFBI, LOX, LOXL1, CYR61, RECK, OLFML2B, BGN, COL1A2, VCAN, LAMC1, COL1A1, JAM2, JAM3, MFAP5, TNC, LUM, COL3A1, ELN, ITGA11, DCN, ITGB3, ITGB1, ABI3BP, VCAM1, LAMB2, CRISPLD2, ITGAV, COL6A3, COL6A2, COL6A1, LAMB1, THBS1, COL8A1, COL8A2, FN1, COL18A1, COL4A2, COL4A1, FBN1, CCDC80, HSPG2, NID1, NID2, SPARC, COL16A1, ECM2, COL5A2, COL5A1, EMILIN1, LAMA2, VWF, LAMA4, FBLN1, COL14A1, ITGA5, FBLN5, PECAM1
BP	GO:0007155	67	16.10577	1.49732E-33	2.56E-30	NUAK1, IGFBP7, POSTN, DDR2, CXCL12, WISP1, SRPX, S1PR1, CTGF, FAP, TGFBI, COL12A1, SPON2, LOXL2, SPON1, CYR61, MPDZ, MFGE8, SSPN, THY1, VCAN, LAMC1, TGFB1I1, COL1A1, MFAP4, ADAM12, PARVA, PLXNC1, CYP1B1, TNC, ITGA11, SPOCK1, ITGB3, ITGBL1, VCAM1, ISLR, LAMB2, ITGAV, COL6A3, COL6A2, COL6A1, COL8A1, THBS1, ENTPD1, LAMB1, THBS2, DPT, FN1, COL18A1, TNXB, SVEP1, COL15A1, NID2, PCDH17, COL16A1, COL5A1, PCDH18, EPHA3, EMILIN1, LAMA2, VWF, LAMA4, OMD, ITGA5, PECAM1, FEZ1, CDH11
BP	GO:0001525	35	8.413462	1.97764E-18	3.39E-15	CYP1B1, ACVRL1, NRP1, LEPR, ELK3, MMP2, MEIS1, MMRN2, S1PR1, CTGF, ITGAV, FAP, TGFBI, TMEM100, COL8A1, COL8A2, FN1, COL18A1, PTPRB, COL4A2, EPAS1, MMP19, HSPG2, COL15A1, MFGE8, MMP14, THY1, PRKD1, SRPX2, MEOX2, ITGA5, CLIC4, PLXDC1, PECAM1, JAM3
BP	GO:0030574	21	5.048077	9.91893E-18	1.7E-14	COL18A1, COL4A2, COL4A1, COL3A1, MMP19, MRC2, COL15A1, MMP14, COL5A2, MMP2, COL5A1, CTSK, COL6A3, COL1A2, COL6A2, COL12A1, COL6A1, COL1A1, COL8A1, ADAMTS2, COL8A2
BP	GO:0030199	17	4.086538	1.23514E-16	1.89E-13	TNXB, CYP1B1, LUM, COL3A1, GREM1, DDR2, COL5A2, COL5A1, COL14A1, SFRP2, COL1A2, COL12A1, COL1A1, LOX, LOXL2, ADAMTS2, DPT
BP	GO:0022617	17	4.086538	1.66779E-11	2.86E-08	A2M, BMP1, FBN1, ELN, MMP19, HSPG2, NID1, DCN, TIMP2, MMP14, MMP2, TIMP1, CTSK, HTRA1, LAMC1, ADAMTS5, FN1
BP	GO:0002576	19	4.567308	2.46966E-11	4.23E-08	RARRES2, A2M, F13A1, TGFB3, IGF1, ACTN1, SERPING1, SPARC, ITGB3, TIMP3, FLNA, TIMP1, ISLR, VWF, CLEC3B, PECAM1, THBS1, CFD, FN1
BP	GO:0042060	15	3.605769	4.08288E-09	6.99E-06	TNC, COL3A1, TGFBR2, TGFB3, SPARC, ELK3, DCN, ITGB3, TPM1, TIMP1, PECAM1, PDGFRA, PDGFRB, LOX, FN1
BP	GO:0035987	10	2.403846	5.93777E-09	1.02E-05	COL4A2, ITGA5, ITGAV, COL12A1, COL6A1, MMP14, COL8A1, LAMB1, MMP2, FN1
BP	GO:0034446	11	2.644231	1.10399E-08	1.89E-05	ITGAV, FERMT2, PEAK1, AXL, LAMC1, ITGB3, ANTXR1, LAMB1, FZD4, FN1, PARVA

Table S6. KEGG pathway analysis of FSTL1 co-expressed genes in GC

GO Term	Number of genes	Associated Genes (%)	Term *P* Value	Term FDR	Associated Genes Found
hsa04512:ECM-receptor interaction	27	6.490384615	2.91E-22	3.54E-19	TNC, COL3A1, ITGA11, ITGB3, ITGB1, LAMB2, ITGAV, COL6A3, COL6A2, COL6A1, THBS1, LAMB1, THBS2, FN1, COL4A2, COL4A1, TNXB, HSPG2, COL5A2, COL5A1, LAMA2, VWF, LAMA4, ITGA5, COL1A2, COL1A1, LAMC1
hsa04510:Focal adhesion	37	8.894230769	6.61E-22	8.05E-19	TNC, COL3A1, ITGA11, ITGB3, ITGB1, MYL9, LAMB2, ITGAV, COL6A3, COL6A2, COL6A1, PDGFC, THBS1, LAMB1, THBS2, AKT3, FN1, COL4A2, TNXB, COL4A1, IGF1, ACTN1, COL5A2, COL5A1, FLNA, LAMA2, VWF, LAMA4, FYN, ITGA5, COL1A2, PDGFRA, PDGFRB, COL1A1, LAMC1, MYLK, PARVA
hsa04151:PI3K-Akt signaling pathway	36	8.653846154	1.32E-13	1.61E-10	TNC, COL3A1, ITGA11, GNG11, LPAR1, ITGB3, ITGB1, LAMB2, ITGAV, COL6A3, COL6A2, COL6A1, PDGFC, THBS1, LAMB1, THBS2, AKT3, CSF1R, FN1, COL4A2, TNXB, COL4A1, IGF1, COL5A2, COL5A1, LAMA2, VWF, LAMA4, ITGA5, COL1A2, PDGFRA, PDGFRB, GNB4, COL1A1, LAMC1, F2R
hsa04974:Protein digestion and absorption	15	3.605769231	1.66E-08	2.02E-05	COL18A1, COL4A2, COL4A1, COL3A1, ELN, COL15A1, COL5A2, COL5A1, COL14A1, COL6A3, COL6A2, COL1A2, COL12A1, COL6A1, COL1A1
hsa05146:Amoebiasis	16	3.846153846	2.59E-08	3.15E-05	COL4A2, IL1R1, COL4A1, COL3A1, TGFB3, ACTN1, COL5A2, COL5A1, LAMA2, LAMA4, LAMB2, COL1A2, COL1A1, LAMC1, LAMB1, FN1
hsa05200:Pathways in cancer	28	6.730769231	5.45E-07	6.63E-04	TGFB3, GNG11, LPAR1, MMP2, ITGB1, CXCL12, EDNRA, LAMB2, ITGAV, LAMB1, AKT3, CSF1R, FN1, COL4A2, COL4A1, EPAS1, TGFBR2, RUNX1T1, IGF1, FZD4, LAMA2, LAMA4, ETS1, PDGFRA, PDGFRB, GNB4, LAMC1, F2R
hsa05410:Hypertrophic cardiomyopathy (HCM)	12	2.884615385	2.10E-06	0.002556	CACNA2D1, ITGA5, ITGAV, TGFB3, ITGA11, SGCD, IGF1, ITGB3, TPM2, TPM1, ITGB1, SGCB
hsa05414:Dilated cardiomyopathy	12	2.884615385	4.43E-06	0.00539	CACNA2D1, ITGA5, ITGAV, TGFB3, ITGA11, SGCD, IGF1, ITGB3, TPM2, TPM1, ITGB1, SGCB
hsa04610:Complement and coagulation cascades	11	2.644230769	4.82E-06	0.005866	PLAT, VWF, A2M, THBD, C3, F13A1, CFH, SERPING1, C1S, CFD, F2R
hsa04611:Platelet activation	14	3.365384615	1.24E-05	0.015151	COL3A1, ITGB3, COL5A2, ITGB1, COL5A1, VWF, PTGIR, FYN, COL1A2, FCGR2A, COL1A1, AKT3, MYLK, F2R
hsa05205:Proteoglycans in cancer	17	4.086538462	2.14E-05	0.026097	LUM, HSPG2, IGF1, DCN, ITGB3, FZD4, TIMP3, ITGB1, MMP2, FLNA, SDC2, ITGA5, ITGAV, MSN, THBS1, AKT3, FN1
hsa05222:Small cell lung cancer	11	2.644230769	3.19E-05	0.038797	LAMA2, COL4A2, LAMA4, COL4A1, LAMB2, ITGAV, LAMC1, LAMB1, ITGB1, AKT3, FN1
hsa05412:Arrhythmogenic right ventricular cardiomyopathy (ARVC)	9	2.163461538	1.81E-04	0.220065	CACNA2D1, ITGA5, ITGAV, ITGA11, SGCD, GJA1, ITGB3, ITGB1, SGCB
hsa04670:Leukocyte transendothelial migration	11	2.644230769	4.09E-04	0.497219	VCAM1, PECAM1, ACTN1, MSN, JAM2, CXCL12, MMP2, JAM3, ITGB1, MYL9, THY1
hsa04810:Regulation of actin cytoskeleton	15	3.605769231	4.87E-04	0.591233	FGD1, ITGA11, ACTN1, ITGB3, ITGB1, MYL9, ITGA5, ITGAV, PDGFRA, PDGFRB, PDGFC, MSN, MYLK, FN1, F2R
hsa04145:Phagosome	12	2.884615385	9.07E-04	1.098218	ITGA5, C3, ITGAV, MRC2, TUBB6, COLEC12, FCGR2A, ITGB3, THBS1, TUBA1A, THBS2, ITGB1
hsa05144:Malaria	7	1.682692308	0.001035	1.252832	VCAM1, LRP1, PECAM1, TGFB3, THBS1, THBS2, SDC2
hsa05206:MicroRNAs in cancer	17	4.086538462	0.00132	1.595565	RECK, TNXB, CYP1B1, TNC, VIM, ZEB2, ITGB3, ZEB1, TPM1, TIMP3, NOTCH3, NOTCH2, ITGA5, PDGFRA, PDGFRB, ZFPM2, THBS1
hsa04360:Axon guidance	10	2.403846154	0.003333	3.983649	PLXNC1, NRP1, FYN, SEMA3C, DPYSL2, CXCL12, ITGB1, SLIT2, EPHA3, SLIT3
hsa04015:Rap1 signaling pathway	12	2.884615385	0.011938	13.60367	PRKD1, PDGFRA, PDGFRB, IGF1, PDGFC, LPAR1, ITGB3, THBS1, ITGB1, AKT3, CSF1R, F2R
hsa05145:Toxoplasmosis	8	1.923076923	0.016227	18.06032	LAMA2, LAMA4, LAMB2, TGFB3, LAMC1, LAMB1, ITGB1, AKT3
hsa04540:Gap junction	7	1.682692308	0.01869	20.52343	PDGFRA, PDGFRB, GJA1, TUBB6, PDGFC, LPAR1, TUBA1A
hsa04514:Cell adhesion molecules (CAMs)	9	2.163461538	0.020532	22.32163	VCAM1, PTPRM, ITGAV, PECAM1, VCAN, JAM2, JAM3, ITGB1, SDC2
hsa04520:Adherens junction	6	1.442307692	0.027304	28.61325	PTPRB, PTPRM, FYN, TGFBR2, ACTN1, SNAI2
hsa04380:Osteoclast differentiation	8	1.923076923	0.037658	37.33436	CTSK, IL1R1, FYN, TGFBR2, FCGR2A, ITGB3, AKT3, CSF1R
hsa05150:Staphylococcus aureus infection	5	1.201923077	0.039915	39.10101	C3, CFH, FCGR2A, C1S, CFD
hsa05202:Transcriptional misregulation in cancer	9	2.163461538	0.047102	44.4251	MAF, PLAT, MEF2C, TGFBR2, RUNX1T1, IGF1, PBX1, MEIS1, CSF1R

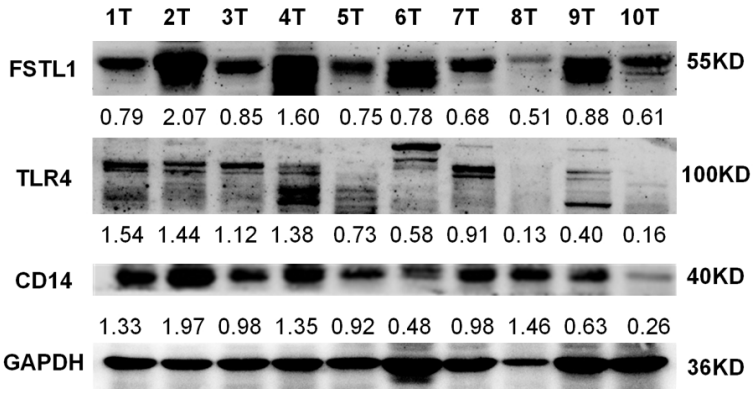

Figure S6. Correlation analysis between TLR4, CD14 expression and FSTL1 level in 10 freshly GC tissues.

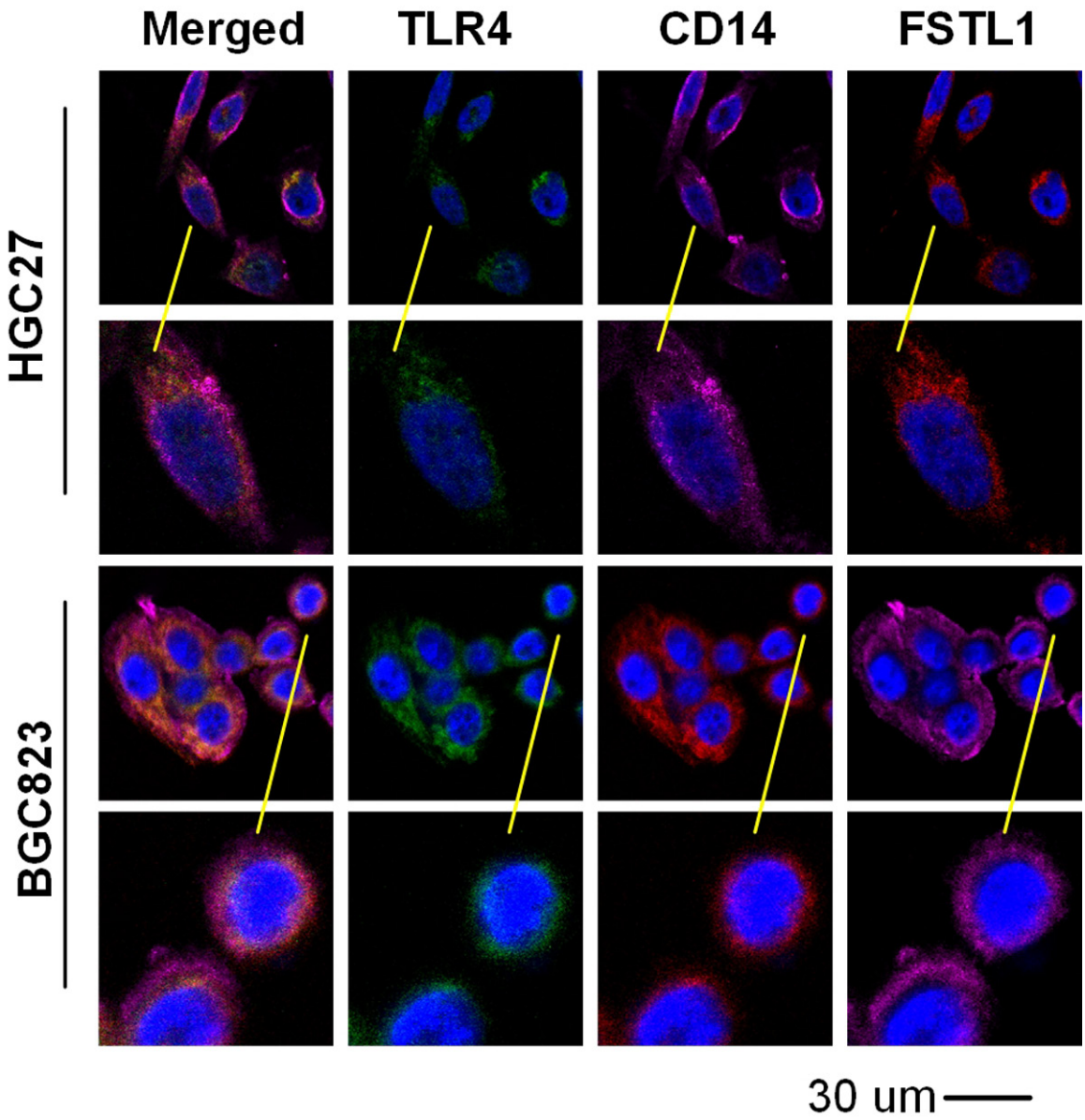

Figure S7. Immunofluorescence images of TLR4, CD14, FSTL1 expression in HGC27 and BGC823 cells.